bioRxiv preprint doi: https://doi.org/10.1101/807792; this version posted October 29, 2019. The copyright holder for this preprint (which was not certified by peer review) is the author/funder, who has granted bioRxiv a license to display the preprint in perpetuity. It is made available under aCC-BY 4.0 International license.

Functionally-informed fine-mapping and polygenic localization of complex trait heritability

Omer Weissbrod[1], Farhad Hormozdiari[1], Christian Benner[2], Ran Cui[3], Jacob Ulirsch[3,4], Steven Gazal[1], Armin P. Schoech[1], Bryce van de Geijn[1], Yakir Reshef[1], Carla Márquez-Luna[5], Luke O'Connor[3], Matti Pirinen[2,6,7], Hilary K. Finucane[3] and Alkes L. Price[1,3]

1. Department of Epidemiology, Harvard T.H. Chan School of Public Health, Boston, MA
2. Institute for Molecular Medicine Finland (FIMM), Helsinki Institute of Life Sciences, University of Helsinki, Helsinki, Finland
3. Program in Medical and Population Genetics, Broad Institute of MIT and Harvard, Cambridge, MA
4. Program in Biological and Biomedical Sciences, Harvard Medical School, Cambridge, MA
5. The Charles Bronfman Institute for Personalized Medicine, Icahn School of Medicine at Mount Sinai, New York, NY
6. Department of Public Health, University of Helsinki, Helsinki, Finland
7. Department of Mathematics and Statistics, University of Helsinki, Helsinki, Finland

Abstract

Fine-mapping aims to identify causal variants impacting complex traits. Several recent methods improve fine-mapping accuracy by prioritizing variants in enriched functional annotations. However, these methods can only use information at genome-wide significant loci (or a small number of functional annotations), severely limiting the benefit of functional data. We propose PolyFun, a computationally scalable framework to improve fine-mapping accuracy using genome-wide functional data for a broad set of coding, conserved, regulatory and LD-related annotations. PolyFun prioritizes variants in enriched functional annotations by specifying prior causal probabilities for fine-mapping methods such as SuSiE or FINEMAP, employing special procedures to ensure robustness to model misspecification and winner's curse. In simulations, PolyFun + SuSiE and PolyFun + FINEMAP were well-calibrated and identified >20% more variants with posterior causal probability >0.95 than their non-functionally informed counterparts (and >33% more fine-mapped variants than previous functionally-informed fine-mapping methods). In analyses of 47 UK Biobank traits (average *N*=317K), PolyFun + SuSiE identified 3,025 fine-mapped variant-trait pairs with posterior causal probability >0.95, a >32% improvement vs. SuSiE; 223 variants were fine-mapped for multiple genetically uncorrelated traits, indicating pervasive pleiotropy. We used posterior mean per-SNP heritabilities from PolyFun + SuSiE to perform polygenic localization, constructing minimal sets of common SNPs causally explaining 50% of common SNP heritability; these sets ranged in size from 28 (hair color) to 3,400 (height) to 550,000 (chronotype). In conclusion, PolyFun prioritizes variants for functional follow-up and provides insights into complex trait architectures.

bioRxiv preprint doi: https://doi.org/10.1101/807792; this version posted October 29, 2019. The copyright holder for this preprint (which was not certified by peer review) is the author/funder, who has granted bioRxiv a license to display the preprint in perpetuity. It is made available under aCC-BY 4.0 International license.

Introduction

Genome-wide association studies of complex traits have been extremely successful in identifying loci harboring causal variants but less successful in fine-mapping the underlying causal variants, making the development of fine-mapping methods a key priority[1,2]. Fine-mapping methods aim to pinpoint causal variants by accounting for linkage disequilibrium (LD) between variants[3–12], but have limited power in the presence of strong LD. One way to increase fine-mapping power is to prioritize variants in functional annotations that are enriched for complex trait heritability[7,8,10,13–17]. However, previous functionally-informed fine-mapping methods such as PAINTOR[18], fastPAINTOR[19], and CAVIARBF[20] have computational limitations and can only use genome-wide significant loci to estimate functional enrichment (and the extension of fGWAS[21] proposed in ref. [10] can only incorporate a small number of functional annotations), severely limiting the benefit of functional data.

We propose PolyFun, a computationally scalable framework for functionally-informed fine-mapping that makes full use of genome-wide data. PolyFun prioritizes variants in enriched functional annotations by defining prior causal probabilities for fine-mapping methods such as SuSiE[22] or FINEMAP[23,24]. PolyFun estimates functional enrichment using a broad set of coding, conserved, regulatory, MAF and LD-related annotations from the baseline-LF model[25–27], aggregating data from across the entire genome and hundreds of functional annotations, via a novel framework that incorporates stratified LD score regression[17] and is robust to modeling misspecification and winner's curse.

We show that PolyFun is well-calibrated and more powerful than previous fine-mapping methods, with a >20% power increase over non-functionally informed fine-mapping methods in simulations. We apply PolyFun to 47 complex traits from the UK Biobank[28] (average N=317K) and identify 3,025 fine-mapped variant-trait pairs with posterior causal probability >0.95, spanning 2,225 unique variants. 223 of these variants were fine-mapped for multiple genetically uncorrelated traits, indicating pervasive pleiotropy. We further used posterior mean per-SNP heritabilities from PolyFun + SuSiE to perform polygenic localization, finding sets of common SNPs causally explaining 50% of common SNP heritability that range in size across many orders of magnitude, from dozens to hundreds of thousands of SNPs.

Results

Overview of methods

PolyFun prioritizes variants in enriched functional annotations by specifying prior causal probabilities in proportion to predicted per-SNP heritabilities and providing them as input to fine-mapping methods such as SuSiE[22]or FINEMAP[23,24]. For each target locus, PolyFun robustly specifies prior causal probabilities for all SNPs on the corresponding odd (resp. even) target chromosome by (1) estimating functional enrichments for a broad set of coding, conserved, regulatory and LD-related annotations from the baseline-LF 2.2.UKB model[26] (187 annotations; Methods, Supplementary Table 1; see URLs) using an L2-regularized extension of S-LDSC[17], restricted to even (resp. odd) chromosomes; (2) estimating per-SNP heritabilities for SNPs on odd (resp. even) chromosomes using the functional enrichment estimates from step 1; (3) partitioning all SNPs into 20 bins of similar estimated per-SNP heritabilities from step 2; (4) re-estimating per-SNP heritabilities for all SNPs on the target chromosome by applying S-LDSC to the 20 bins, restricted to odd (resp. even) chromosomes excluding the target chromosome; and (5) setting prior causal probabilities for SNPs on the target chromosome proportional to per-SNP heritabilities from step 4. The

bioRxiv preprint doi: https://doi.org/10.1101/807792; this version posted October 29, 2019. The copyright holder for this preprint (which was not certified by peer review) is the author/funder, who has granted bioRxiv a license to display the preprint in perpetuity. It is made available under aCC-BY 4.0 International license.

L2 regularization in step 1 improves the accuracy of per-SNP heritability estimation; the partitioning into odd and even chromosomes in steps 1-2 and the exclusion of the target chromosome in step 4 prevents winner's curse; and the re-estimation of per-SNP heritabilities in step 4 ensures robustness to model misspecification.

PolyFun specifies prior causal probabilities in proportion to per-SNP heritability estimates:

$$\mathrm{P}(\beta_i \neq 0 | \boldsymbol{a}_i) \propto \mathrm{var}[\beta_i | \boldsymbol{a}_i], \qquad (1)$$

where β_i is the causal effect size of SNP i in standardized units (the number of standard deviations increase in phenotype per 1 standard deviation increase in genotype), $\boldsymbol{a}_i$ is the vector of functional annotations of SNP i, and $\mathrm{var}[\beta_i | \boldsymbol{a}_i]$ is the estimated per-SNP heritability of SNP i from step 4 (see above). Equation 1 is derived by applying the law of total variance to $\mathrm{var}[\beta_i | \boldsymbol{a}_i]$, assuming that SNP effect sizes are sampled from a mixture distribution and that functional enrichment is primarily due to differences in polygenicity, motivated by our recent work[29] (see Methods).

A key distinction between PolyFun and previous functionally-informed fine-mapping methods[10,18–20] is the use of the entire genome and a large number of functional annotations to estimate prior causal probabilities. PolyFun achieves this by decoupling functional enrichment estimation and fine-mapping, which allows rapidly pooling data across millions of SNPs and >100 functional annotations from the baseline-LF model (see Methods). In contrast, previous functionally-informed fine-mapping methods can only aggregate information across a small number of loci (e.g. genome-wide significant loci)[18–20] or a small number of functional annotations[10] due to computational limitations. We exploited the computational scalability of PolyFun (together with SuSiE[22]) to fine-map up to 2,763 overlapping 3Mb loci spanning the entire genome (excluding loci with close to zero heritability; Methods), instead of only analyzing genome-wide significant loci. We subsequently used our fine-mapping results to perform polygenic localization, identifying minimal sets of common SNPs causally explaining a given proportion of common SNP heritability. Details of the PolyFun method are provided in the Methods section; we have released open-source software implementing PolyFun in conjunction with SuSiE[22] and FINEMAP[23] (see URLs). In all analyses in this manuscript, we applied PolyFun using summary LD information estimated directly from the target samples (both for running S-LDSC and for running SuSiE or FINEMAP), as previously recommended for fine-mapping methods[12,30].

Simulations

We evaluated PolyFun via simulations using real genotypes from 337,491 unrelated UK Biobank samples of British ancestry[28]. We analyzed 10 3Mb loci (following previous recommendations on fine-mapping locus size[12]) on chromosome 1 with different SNP densities, each containing 1,468-27,784 imputed MAF≥0.001 SNPs (including short indels; Supplementary Table 2). We estimated prior causal probabilities using 18,212,157 genome-wide imputed MAF≥0.001 SNPs with INFO score≥0.6 (excluding three long-range LD regions; see Methods). We simulated traits with heritability equal to 25% and genome-wide proportion of causal SNPs equal to 0.5%, with the target locus in each simulation including 10 causal SNPs jointly explaining heritability equal to 0.05%. To define prior causal probabilities for the generative model, we generated a per-SNP heritability for every SNP based on its LD, MAF, and functional annotations, using the baseline-LF model[26] with meta-analyzed functional enrichments from analyses of real data (Supplementary Table 3), and then defined causal probabilities in proportion to these per-SNP heritabilities (Equation 1; Methods). We sampled causal SNPs based on these causal probabilities, sampled causal effect sizes from the same normal distribution for each causal SNP (motivated by our

bioRxiv preprint doi: https://doi.org/10.1101/807792; this version posted October 29, 2019. The copyright holder for this preprint (which was not certified by peer review) is the author/funder, who has granted bioRxiv a license to display the preprint in perpetuity. It is made available under aCC-BY 4.0 International license.

recent work[29]), and generated summary statistics with sampling noise based on *N*=320K samples (corresponding to a 95% phenotyping rate for N=337K samples) using summary LD information from the same samples. Other parameter settings were explored in secondary analyses (see below). Further details of the simulation framework are provided in the Methods section.

We evaluated 10 fine-mapping methods (Table 1): fastPAINTOR−, fastPAINTOR, CAVIARBF1−, CAVIARBF1, CAVIARBF2−, CAVIARBF2, FINEMAP, PolyFun + FINEMAP, SuSiE, and PolyFun + SuSiE. (We did not evaluate methods that do not incorporate functional annotations or prior causal probabilities, such as CAVIAR[5].) For each method, we used summary LD information estimated directly from the target samples, as in our analyses of real traits. For fastPAINTOR−, fastPAINTOR, SuSiE, and PolyFun + SuSiE, we specified a per-locus causal effect size variance ($\mathrm{var}[\beta_i|\beta_i \neq 0]$) using a causal effect size variance estimator that we implemented, which yielded improved results over the default estimator implemented in these methods (see Methods). We ran fastPAINTOR with 10 annotations that we selected to maximize power while maintaining correct calibration (Methods). We used default settings for all other parameters, except as otherwise indicated. We applied fastPAINTOR, CAVIARBF1, and CAVIARBF2 to one locus at a time due to computational limitations (see below). Results for FINEMAP, PolyFun + FINEMAP, SuSiE, and PolyFun + SuSiE were averaged across 1,000 simulations, and results for other methods were averaged across 100 simulations due to computational limitations.

We assessed calibration via the proportion of false positives among SNPs with posterior causal probability (posterior inclusion probability; PIP) above a given threshold (e.g. PIP>0.95 or PIP>0.5), aggregating the results across all simulations; we refer to this quantity as the false discovery rate (although we do not use frequentist false discovery rate methods[31,32]). For each PIP threshold, we conservatively estimated false discovery rates by setting all PIPs greater than the threshold to the threshold, yielding a uniform false-discovery threshold (Methods, Figure 1a-b, Supplementary Figure 1a-b, Supplementary Table 4); exact false-discovery thresholds are reported in Supplementary Figure 1a-b and Supplementary Table 4. No method except CAVIARBF2- and CAVIARBF2 had significantly inflated false discovery rates, although fastPAINTOR and CAVIARBF1 had suggestive evidence of inflated false discovery rates (due to high computational costs, we did not perform enough simulations to determine if this miscalibration was statistically significant). CAVIARBF2− and CAVIARBF2 had severely inflated false discovery rates at multiple PIP cutoffs (Supplementary Table 4), contrary to expectations as modeling multiple causal variants is advantageous in most settings[3]. Similarly, no method had a significantly inflated false discovery rate at the PIP>0.95 threshold when using exact false-discovery thresholds, although all methods had inflated false discovery rates at the PIP>0.5 threshold with exact false-discovery thresholds (significant for methods for which we ran 1,000 simulations), demonstrating the challenges of exact calibration in fine-mapping (Supplementary Figure 1, Table 4).

We assessed power via the proportion of true causal SNPs with PIP above a given threshold, aggregating the results across all simulations (Figure 1c-d, Supplementary Table 4). PolyFun + FINEMAP was the most powerful method, identifying >5% more PIP>0.95 causal SNPs than PolyFun + SuSiE and >20% more PIP>0.95 causal SNPs than FINEMAP (Supplementary Table 4). PolyFun + SuSiE was the second most powerful method, identifying >25% more PIP>0.95 causal SNPs than SuSiE. PolyFun + FINEMAP and PolyFun + SuSiE were equally powerful at PIP>0.5, identifying >37% more PIP>0.5 causal SNPs than all other methods. These results demonstrate the benefits of using functional annotations for SNP prioritization. We note that power to identify PIP>0.95 or PIP>0.5 SNPs is generally expected to be low

bioRxiv preprint doi: https://doi.org/10.1101/807792; this version posted October 29, 2019. The copyright holder for this preprint (which was not certified by peer review) is the author/funder, who has granted bioRxiv a license to display the preprint in perpetuity. It is made available under aCC-BY 4.0 International license.

(on the order of 10% or lower), as fine-mapping is a statistically hard problem due to pervasive LD[3]. However, power was substantially higher at lower PIP thresholds (Supplementary Table 4).

We evaluated the computational cost of each method. SuSiE and PolyFun + SuSiE were much faster than the other methods, fine-mapping a 3Mb locus in 5 minutes on average (excluding fixed preprocessing time; see below), compared with 227 minutes for fastPAINTOR−, 235 minutes for fastPAINTOR, 20 minutes for CAVIARBF1−, 34 minutes for CAVIARBF1, 70 minutes for CAVIARBF2−, 84 minutes for CAVIARBF2, 14 minutes for FINEMAP, and 17 minutes for PolyFun + FINEMAP (Figure 2a, Supplementary Table 4). CAVIARBF methods allowing >2 causal SNPs per locus were not evaluated because they typically required >48 hours for a single analysis. We note that the computational costs for fastPAINTOR, CAVIARBF1, and CAVIARBF2 that we report here for 3Mb loci are larger than those previously reported for smaller loci (typically ≤100kb)[18–20]. PolyFun also requires fixed preprocessing time (steps 1-4; see Overview of methods) of 630 minutes on average (equivalent to 0.2 minutes per locus in a genome-wide analysis); when restricting analyses to subsets of loci, PolyFun + SuSiE was still faster than all other functionally-informed methods when analyzing >23 loci (Figure 2b).

To assess the robustness of PolyFun to model misspecification of functional architectures (i.e. generative models of causal effect sizes as a function of functional annotations), we also simulated data using two functional architectures that are different from the additive functional architecture assumed by S-LDSC with the baseline-LF model[26]: (i) a multiplicative functional architecture in which per-SNP heritabilities are proportional to a product of terms for each annotation[21,33], and (ii) a sub-additive functional architecture in which per-SNP heritabilities are proportional to a maximum of terms for each annotation (see Methods). In both cases, PolyFun + SuSiE and PolyFun + FINEMAP remained well-calibrated and attained a >24% increase in power over the respective non-functionally informed methods (Supplementary Table 4). On the other hand, alternative functionally-informed extensions of SuSiE and FINEMAP that specify prior causal probabilities (Equation 1) in proportion to standard S-LDSC per-SNP heritability estimates or to L2-regularized S-LDSC per-SNP heritability estimates (the output of step 1 of PolyFun) suffered inflated false discovery rates or reduced power (Supplementary Table 4), demonstrating the importance of robustly specifying prior causal probabilities.

We performed 9 secondary analyses. First, we evaluated 95% credible sets, defined as sets with probability >0.95 of including ≥1 causal SNP(s)[22] (this is different from an earlier definition of 95% credible set as the smallest set of SNPs accounting for 95% of the posterior probability[4,5,18]); we note that 95% credible sets generally contain many non-causal SNPs. The union of PolyFun + SuSiE credible sets included 25 SNPs on average (27% fewer than SuSiE) and spanned 22% of the true causal SNPs (1% more than SuSiE) (Supplementary Table 4). The union of PolyFun + FINEMAP 95% credible sets included 27 SNPs on average (27% fewer than FINEMAP) and spanned 27% of the true causal SNPs (5% more than FINEMAP) (Supplementary Table 4). Second, we evaluated the methods under different simulated sample sizes. The relative power advantage of PolyFun + SuSiE over SuSiE (resp. PolyFun + FINEMAP over FINEMAP) at a PIP>0.95 threshold was equal to 22% (resp. 14%) at N=1 million, vs. 25% (resp. 20%) at N=320K (corresponding to the typical number of phenotyped individuals in the full UK Biobank), with a roughly linear increase in absolute power (Supplementary Table 4). These results indicate that functionally informed fine-mapping remains valuable at substantially larger sample sizes. Third, we verified that the improvement of PolyFun remained qualitatively similar for different values of the number of causal SNPs per target locus (Supplementary Table 4) or the heritability causally explained by the target locus (Supplementary Table 4). Fourth, we verified that the improvement of PolyFun remained qualitatively

bioRxiv preprint doi: https://doi.org/10.1101/807792; this version posted October 29, 2019. The copyright holder for this preprint (which was not certified by peer review) is the author/funder, who has granted bioRxiv a license to display the preprint in perpetuity. It is made available under aCC-BY 4.0 International license.

similar for different values of genome-wide polygenicity (Supplementary Table 4) and genome-wide heritability (Supplementary Table 4). Fifth, we verified that the improvement of PolyFun remained qualitatively similar when changing the maximum number of causal SNPs modeled by PolyFun + SuSiE and PolyFun + FINEMAP from 10 to 1-5 (Supplementary Table 4). Sixth, for all methods not based on CAVIARBF, we compared the performance of our per-locus causal effect size variance estimator to the default estimators (CAVIARBF-based methods perform fine-mapping using several prespecified values and then average the results[20]). We determined that the false discovery rate of fastPAINTOR-, fastPAINTOR, SuSiE and PolyFun + SuSiE improved when using our estimator (Supplementary Table 4). On the other hand, for FINEMAP and PolyFun + FINEMAP, causal discovery rate and power remained similar when using our estimator, but the sizes of 95% credible set sizes increased substantially (Supplementary Table 4), and thus we used the default FINEMAP estimator in all primary analyses. Seventh, we verified that fastPAINTOR performance was approximately optimized when incorporating 10 functional annotations (selected to maximize power while maintaining correct calibration, see Methods) (Supplementary Table 4). Eighth, we determined that the false discovery rate of PolyFun increased when using unregularized S-LDSC in step 1 of PolyFun, demonstrating the importance of regularization for functionally-informed fine-mapping (Supplementary Table 4). Finally, we evaluated fine-mapping performance when specifying the true prior causal probabilities that we used to generate the data, a "cheating" method, and determined that this substantially reduced the false discovery rate and increased the power of PolyFun + SuSiE and PolyFun + FINEMAP (Supplementary Table 4), confirming that more accurate prior causal probabilities lead to more powerful fine-mapping.

We conclude from these experiments that PolyFun + FINEMAP and PolyFun + SuSiE outperformed all other methods, with a 3.4x faster runtime for PolyFun + SuSiE; fastPAINTOR−, fastPAINTOR, CAVIARBF1− and CAVIARBF1 had lower power and high computational costs; CAVIARBF2- and CAVIARBF2 had extremely inflated false discovery rates; and CAVIARBF methods allowing >2 causal SNPs per locus had prohibitive computational costs. (We note that the power of fastPAINTOR, CAVIARBF1, and CAVIARBF2 could potentially be improved by jointly fine-mapping multiple genome-wide significant loci, but the computational costs would be prohibitive when there are many such loci.) Thus, we restricted our analysis of real traits to SuSiE and PolyFun + SuSiE.

Functionally informed fine-mapping of 47 complex traits in the UK Biobank

We applied PolyFun + SuSiE to fine-map 47 traits in the UK Biobank, including 31 traits analyzed in refs. [34,35], 9 blood cell traits analyzed in ref. [12], and 7 recently released metabolic traits (average N=317K; Supplementary Table 5). For each trait we fine-mapped up to 2,763 overlapping 3Mb loci spanning M=18,212,157 imputed MAF≥0.001 SNPs with INFO score≥0.6 (including short indels; excluding three long-range LD regions and loci with close to zero heritability; Methods). We assigned to each SNP its PIP computed using the locus in which it was most central. We have publicly released the PIPs and the prior and posterior means and variances of the causal effect sizes for all SNPs and traits analyzed (see URLs).

PolyFun + SuSiE identified 3,025 PIP>0.95 fine-mapped SNP-trait pairs, a >32% improvement vs. SuSiE; 9,670 PIP>0.5 SNP-trait pairs, a >59% improvement vs. SuSiE; and 222,842 PIP>0.05 SNP-trait pairs, a >83% improvement vs. SuSiE (Supplementary Table 6). The number of PIP>0.95 SNPs per trait ranged from 2 (neuroticism) to 407 (height) (Figure 3a, Supplementary Table 6). The 3,025 PIP>0.95 SNP-trait pairs spanned 2,225 unique SNPs, including 532 low-frequency SNPs (0.005<MAF<0.05) and 185 rare SNPs

bioRxiv preprint doi: https://doi.org/10.1101/807792; this version posted October 29, 2019. The copyright holder for this preprint (which was not certified by peer review) is the author/funder, who has granted bioRxiv a license to display the preprint in perpetuity. It is made available under aCC-BY 4.0 International license.

(0.001<MAF<0.005) (Supplementary Table 7). Only 39% of the 2,225 PIP>0.95 SNPs were also lead GWAS SNPs (defined as MAF>0.001 SNPs with $P<5\times10^{-8}$ and no MAF>0.001 SNP with a smaller p-value within 1Mb) (Supplementary Table 7), demonstrating the importance of using fine-mapped SNPs rather than lead GWAS SNPs for downstream analysis. 31% of the PIP>0.95 SNPs resided in coding regions and 22% were non-synonymous (broadly consistent with previous fine-mapping studies[8,12]) (Supplementary Table 7). When restricting the analysis to 15 genetically uncorrelated traits ($|r_g|<0.2$; Methods and Supplementary Tables 8-9) we identified 1,626 PIP>0.95 SNP-trait pairs spanning 1,496 unique SNPs, with a median distance of 9kb between a PIP>0.95 SNP and the nearest lead GWAS SNP for the same trait (Supplementary Table 7). The 15 genetically uncorrelated traits included 5,306 genome-wide significant locus-trait pairs (defined by 1Mb windows around lead GWAS SNPs) harboring 0.28 PIP>0.95 SNPs per locus on average (Supplementary Table 10); 9% of the PIP>0.95 SNP-trait pairs did not lie within genome-wide significant loci. 1,080 of the 5,306 locus-trait pairs (20%) harbored ≥1 PIP>0.95 SNP(s), harboring 1.37 PIP>0.95 SNPs on average (Supplementary Table 10).

We estimated the SNP-heritability (h_g^2) tagged by PIP>0.95 fine-mapped SNPs (which is likely to be close to the heritability causally explained by these SNPs, if most of the tagged SNP-heritability originates from PIP>0.95 SNPs). The h_g^2 tagged by PIP>0.95 SNPs captured a large proportion of the h_g^2 tagged by lead GWAS SNPs (median proportion=52%; Figure 3b, Methods, Supplementary Table 11). This proportion was substantially larger than the proportion of GWAS loci harboring PIP>0.95 SNPs (20%; see above), as fine-mapping power is higher at loci with larger causal effects (Supplementary Table 4). However, fine-mapped SNPs tagged a smaller proportion of total MAF>0.001 h_g^2 (median proportion=21%; Figure 3b, Methods, Supplementary Table 11), indicating that substantially larger sample sizes are required to comprehensively fine-map all heritable SNP effects.

Among the 2,225 unique PIP>0.95 SNPs fine-mapped for at least one trait, 223 SNPs were fine-mapped for multiple genetically uncorrelated traits (selecting a different subset of genetically uncorrelated traits for each SNP; Methods), including 55 SNPs fine-mapped for ≥3 genetically uncorrelated traits, indicating pervasive pleiotropy (Figure 4, Supplementary Table 12). 118 pleiotropic SNPs resided in coding regions and 93 were non-synonymous (Supplementary Table 12). The 17 SNPs fine-mapped for at least 4 traits are reported in Table 2. Top pleiotropic SNPs included (1) rs13107325, a non-synonymous SNP in the gene SLC39A8, which was fine-mapped for balding, BMI, diastolic blood pressure, forced vital capacity, height, red blood cell count, total cholesterol, and waist hip ratio (adjusted for BMI); (2) rs1229984, a non-synonymous SNP in the gene ADH1B, which was fine-mapped for BMI, LDL, mean corpuscular hemoglobin, mean platelet volume, systolic blood pressure, total cholesterol, and Vitamin D; and (3) rs76895963, a conserved intronic SNP in a promoter of the gene CCND2, which was fine-mapped for bone mineral density, height, red blood cell count, systolic blood pressure and triglycerides. The gene SLC39A8 is a zinc transporter and is associated with congenital disorder of glycosylation[36,37]; the gene ADH1B is an alcohol dehydrogenase gene and is associated with alcohol dependence[38]; and the gene CCND2 participates in cell cycle regulation and is associated with delayed psychomotor development[39]. We note that previous studies have reported that genetically uncorrelated traits often share association signals at the same loci[40], but did not fine-map those signals to individual SNPs as performed here.

To better understand the improvement of PolyFun + SuSiE over SuSiE, we examined the 121 loci where PolyFun + SuSiE identified a fine-mapped common SNP (PIP>0.95) but SuSiE did not (PIP<0.5 for all SNPs within 1Mb) (Figure 5 and Supplementary Table 13). In each case, functional annotations prioritized one

bioRxiv preprint doi: https://doi.org/10.1101/807792; this version posted October 29, 2019. The copyright holder for this preprint (which was not certified by peer review) is the author/funder, who has granted bioRxiv a license to display the preprint in perpetuity. It is made available under aCC-BY 4.0 International license.

SNP out of several candidates, greatly improving fine-mapping resolution. Examples included (a) height, for which rs288326, a non-synonymous SNP, had PIP=0.96 for PolyFun + SuSiE vs. PIP=0.35 for SuSiE (Figure 5a); (b) BMI, for which rs12330631, a conserved SNP, had PIP=0.96 for PolyFun + SuSiE vs. PIP=0.25 for SuSiE (Figure 5b); (c) red blood cell count, for which rs80207740, a promoter SNP, had PIP=0.97 for PolyFun + SuSiE vs. PIP=0.28 for SuSiE (Figure 5c); and (d) platelet count, for which rs2270894, a promoter SNP, had PIP=0.96 for PolyFun + SuSiE vs. PIP=0.19 for SuSiE (Figure 5d). Results for all 121 loci are reported in Supplementary Table 13.

We validated the motivation for performing functionally-informed fine-mapping by verifying that fine-mapped SNPs are enriched for functional annotations, as previously shown for autoimmune diseases[7,8,10] and blood traits[12]. We used non-functionally-informed SuSiE in this analysis to avoid biasing the results. For each of 50 main binary annotations from the baseline-LF model[25], for various PIP ranges, we computed the functional enrichment of fine-mapped common SNPs in the PIP range, defined as the proportion of common SNPs in the PIP range lying in the annotation divided by the proportion of genome-wide common SNPs lying in the annotation, and meta-analyzed the results across genetically uncorrelated traits (Methods, Figure 6, Supplementary Table 14). PIP>0.95 SNPs were strongly and significantly enriched for non-synonymous SNPs (51x enrichment, $P=6.8\times10^{-185}$) and SNPs in conserved regions (16x enrichment, $P<10^{-300}$), significantly enriched for SNPs in various regulatory annotations (e.g. promoter-ExAC and H3K4me3), and significantly depleted for SNPs in repressed regions, consistent with previous literature on functional enrichment of fine-mapped SNPs[7,8,10–12] and disease heritability[17,25,26,41]. We observed qualitatively similar but weaker enrichments at lower PIP ranges (Figure 6, Supplementary Table 14).

We compared our fine-mapping results to two previous studies. First, we compared our results to ref. [12], which performed non-functionally informed fine-mapping (using a previous version of FINEMAP[23]) for the 9 blood cell traits using a subset of approximately 115K of the individuals included in our analyses. PolyFun + SuSiE identified 1,268 PIP>0.95 SNP-trait pairs (4.4× more than ref. [12]; 289 PIP>0.95 SNP-trait pairs), 146 of which were shared (PIP>0.95) across the two studies, including all four SNPs that were functionally validated via luciferase reporter assays in ref. [12] (PIP>0.999 for all four SNPs; Methods, Supplementary Tables 15-17). Sample size was the most important difference between the two studies, and incorporation of functional priors was also important, as we determined that (non-functionally informed) SuSiE identified only 984 PIP>0.95 SNP-trait pairs (3.4x more than ref. [12]), 146 of which were shared (Supplementary Tables 15-16). Surprisingly, many differences remained even after we restricted SuSiE to the same subset of 115K individuals analyzed in ref. [12] (242 PIP>0.95 SNP-trait pairs, 130 of which were shared; Supplementary Tables 15-16), possibly due to differences in the underlying methods, data preprocessing, or reference panel used to impute genotypes. Second, we compared our results to ref. [7], which performed non-functionally-informed fine-mapping for 7 of our traits (bone mineral density, fasting glucose, HDL cholesterol, LDL cholesterol, platelet count, red blood cell count, triglycerides), using a non-functionally informed method (PICS) and independent smaller data sets. PolyFun + SuSiE identified 727 PIP>0.95 SNP-trait pairs (35x more than ref. [7]; 21 PIP>0.95 SNP-trait pairs; Supplementary Tables 18-19). 12 SNP-trait pairs had PIP>0.95 in both studies, implying a replication rate (in independent data) of 57% (12/21) in our study. We caution that the fine-mapping power of PolyFun + SuSiE is likely much lower than 57% in practice, because the 21 SNPs fine-mapped in ref. [7] are likely to have larger effect sizes than most causal SNPs. We did not compare our results to refs. [8,10,11] because those studies analyzed disease traits, for which the number of cases in the UK Biobank is relatively low.

bioRxiv preprint doi: https://doi.org/10.1101/807792; this version posted October 29, 2019. The copyright holder for this preprint (which was not certified by peer review) is the author/funder, who has granted bioRxiv a license to display the preprint in perpetuity. It is made available under aCC-BY 4.0 International license.

We performed 5 secondary analyses. First, we verified the robustness of our fine-mapping results by repeating the analysis using data from only the UK Biobank interim release (average *N*=107K) for the five traits with highest fine-mapping power (Methods): height, platelet count, bone mineral density, red blood cell count, and lymphocyte count. PolyFun + SuSiE identified >45% more PIP>0.95 SNPs vs. SuSiE overall, and >33% more PIP>0.95 SNPs vs. SuSiE among SNPs having PIP>0.95 in the full *N*=337K SuSiE results, with a similar rate of replication in the full *N*=337K SuSiE results (Supplementary Table 20). Second, in the *N*=337K analysis, we determined that the union of PolyFun + SuSiE 95% credible sets (defined as sets with probability >0.95 of including ≥1 causal SNP[22]; see above) was 23% smaller than the union of SuSiE 95% credible sets (median reduction) (Supplementary Table 21), consistent with simulations (Supplementary Table 4). Third, we searched for pairs of fine-mapped SNPs within 1Mb of each other where exactly one of the SNPs is coding, which can aid in linking regulatory variants to target genes[42–44], and identified 490 such pairs (Supplementary Table 22). Fourth, we compared the magnitude of the posterior mean and posterior standard deviation of causal effect sizes, which can inform the applicability of fine-mapping results to polygenic risk scores. Posterior means were 3.6x smaller than posterior standard deviations (median ratio) for PIP>0.05 SNPs but 6.9x larger for PIP>0.95 SNPs, for which causal effect sizes are estimated with high accuracy (Supplementary Table 7). Fifth, we verified that the functional enrichments of fine-mapped SNPs remained qualitatively similar when using PolyFun + SuSiE instead of SuSiE (Supplementary Figure 2, Supplementary Table 23) and when defined using all MAF≥0.001 SNPs (Supplementary Figure 3, Supplementary Table 24) or only low-frequency and rare SNPs (0.05>MAF≥0.001) (Supplementary Figure 4, Supplementary Table 25).

In summary, we leveraged the improved power of PolyFun + SuSiE to robustly identify thousands of fine-mapped SNPs, providing a rich set of potential candidates for functional follow-up. Our results further indicate pervasive pleiotropy, with many SNPs fine-mapped for two or more genetically uncorrelated traits.

Functionally-informed polygenic localization of 47 complex traits in the UK Biobank

PIP>0.95 SNPs tag a large proportion of the SNP-heritability (h_g^2) tagged by lead GWAS SNPs (median proportion=52%) but a small proportion of total genome-wide h_g^2 (median proportion=21%) (Figure 3b), implying that they causally explain a small proportion of h_g^2. We thus propose *polygenic localization*, whose aim is to identify a minimal set of common SNPs causally explaining a specified proportion of common SNP heritability. A key difference between polygenic localization and previous studies of polygenicity[29,45–48] is that polygenic localization aims to *identify* (not just characterize) such SNPs.

Given a ranking of SNPs by posterior per-SNP heritability (i.e., the posterior mean of their squared effect size; see Methods), we define $M_{50\%}$ as the size of the smallest set of top-ranked common SNPs causally explaining 50% of common SNP heritability (resp. M_p for proportion p of common SNP heritability). We estimate $M_{50\%}$ (resp. M_p) by (1) partitioning SNPs into 50 ranked bins of similar posterior per-SNP heritability estimates from PolyFun + SuSiE and stratifying the lowest-heritability bin into 10 equally-sized MAF bins, yielding 59 bins; (2) running S-LDSC using a different set of samples to re-estimate the average per-SNP heritability in each bin; and (3) computing the number of top-ranked common SNPs (with respect to the original ranking) whose estimated per-SNP heritabilities (from step 2) sum up to 50% (resp. the proportion p) of the total estimated SNP-heritability. We refer to this method as PolyLoc. The analysis of new samples in step 2 of PolyLoc prevents winner's curse; although PolyFun + SuSiE is robust to winner's

bioRxiv preprint doi: https://doi.org/10.1101/807792; this version posted October 29, 2019. The copyright holder for this preprint (which was not certified by peer review) is the author/funder, who has granted bioRxiv a license to display the preprint in perpetuity. It is made available under aCC-BY 4.0 International license.

curse, PolyLoc would be susceptible to winner's curse if it reused the data analyzed by PolyFun + SuSiE. We note that $M_{50\%}$ relies on an empirical ranking and is thus larger than the size of the smallest set of SNPs causally explaining 50% of common SNP heritability, denoted as $M^*_{50\%}$ ($M_{50\%} \geq M^*_{50\%}$). We further note that PolyLoc will yield robust estimates of $M_{50\%}$ if S-LDSC yields robust estimates of the SNP-heritability causally explained by each bin. Although S-LDSC has previously been shown to produce robust estimates[17,25–27], we performed extensive simulations to confirm that PolyLoc produced robust estimates of $M_{50\%}$ (Methods, Supplementary Tables 29-30). Further details of PolyLoc are provided in the Methods section; we have released open source software implementing PolyLoc (see URLs).

We applied PolyLoc to the 47 complex traits from the UK Biobank (Supplementary Table 5). We ranked SNPs using *N*=337K unrelated British ancestry samples (steps 1-2) and re-estimated average per-SNP heritabilities in each of 59 SNP bins using S-LDSC applied to *N*=122K European-ancestry UK Biobank samples that were not included in the *N*=337K set (step 3). Estimates of $M_{50\%}$ ranged widely from 28 (hair color) to 3.4K (height) to 553K (chronotype, or morning person; Figure 7, Supplementary Table 26). The median estimate of $M_{50\%}$ across 15 genetically uncorrelated traits was 3.4K; the median estimate of $M_{5\%}$ was 7; and the median estimate of $M_{95\%}$ was 4.3 million (of 7.0 million total common SNPs) (Supplementary Table 26). We verified that $M_{50\%}$ estimates were strongly correlated with estimates of the effective number of independently associated SNPs (M_e; ref. [29]), with log-scale r=0.88 (P=6.2×10^{-5}) across 13 genetically uncorrelated traits with published M_e estimates (Supplementary Table 27); as noted above, PolyLoc provides the SNP sets underlying its estimates, unlike ref. [29].

We performed 6 secondary analyses. First, we used posterior per-SNP heritability estimates from SuSiE (instead of PolyFun + SuSiE) to partition SNPs into heritability bins, obtaining $M_{50\%}$ estimates that were 1.4x larger (median ratio; Supplementary Table 28). This result is consistent with our results showing that PolyFun + SuSiE identifies more PIP>0.95, PIP>0.5 and PIP>0.05 SNPs than SuSiE (Supplementary Table 6), and further illustrates the improved fine-mapping resolution of PolyFun + SuSiE vs. SuSiE. Second, we applied PolyLoc to *prior* estimates of per-SNP heritability computed by S-LDSC based only on functional annotations (including MAF bins; Methods) and obtained $M_{50\%}$ estimates that were overwhelmingly larger, emphasizing the value of posterior estimates (Supplementary Table 28). Third, we modified PolyLoc by applying step (3) of PolyLoc to the same *N*=337K samples analyzed by PolyFun + SuSiE. We obtained $M_{50\%}$ estimates that were drastically different, a consequence of winner's curse (Supplementary Table 28). Fourth, we verified that PolyLoc results were not sensitive to the number of heritability bins (Supplementary Table 28). Fifth, we determined that polygenic localization estimates were slightly larger when not stratifying the lowest-heritability bin into 10 MAF bins (Supplementary Table 28). Sixth, We determined that $M_{50\%}$ estimates using all MAF≥0.001 SNPs were 1.4x larger (vs. 2.8x larger SNP set) compared to analyses of common SNPs, confirming that rare and low-frequency SNPs are depleted for high-heritability SNPs[26,45,49] (Supplementary Table 28).

Our results demonstrate that half of the common SNP heritability of complex traits is causally explained by typically thousands of SNPs (median $M_{50\%}$=3.4K), and the remaining heritability is spread across an extremely large number of extremely weak-effect SNPs (median $M_{95\%}$=4.3 million), consistent with extremely polygenic but heavy-tailed trait architectures[1,29,45,46,50–54].

bioRxiv preprint doi: https://doi.org/10.1101/807792; this version posted October 29, 2019. The copyright holder for this preprint (which was not certified by peer review) is the author/funder, who has granted bioRxiv a license to display the preprint in perpetuity. It is made available under aCC-BY 4.0 International license.

Discussion

We have introduced PolyFun, a framework that improves fine-mapping by prioritizing variants that are a-priori more likely to be causal based on their functional annotations. Across 47 UK Biobank traits, PolyFun + SuSiE confidently fine-mapped 3,025 SNP-trait pairs (PIP >0.95), a 32% increase over non-functionally informed SuSiE. The fine-mapped SNPs span 20% of GWAS loci but explain 52% of lead GWAS SNP-heritability, as fine-mapping power is higher at loci with larger causal effects. 223 of the fine-mapped SNPs were fine-mapped for multiple genetically uncorrelated traits, indicating pervasive pleiotropy. PolyFun improves our ability to scale the identification of causal variants underlying association signals, a primary challenge in genetics research[2]. We further leveraged the results of PolyFun to perform polygenic localization by constructing minimal SNP sets causally explaining a given proportion of common SNP heritability, demonstrating that 50% of common SNP heritability can be explained by sets ranging in size from 28 (hair color) to 3,400 (height) to 550,000 (chronotype). We have publicly released the PIPs and the prior and posterior means and variances of effect sizes for all SNPs and traits analyzed (see URLs).

Our results provide several opportunities for future work. First, the fine-mapped SNPs that we have identified can be prioritized for functional follow-up. Second, fine-mapping results (posterior mean effect sizes) can be used to compute polygenic risk scores[55]. This may be especially useful for cross-population prediction, which is sensitive to misspecification of causal SNPs due to LD differences between populations[56,57]. Third, the proximal pairs of coding and non-coding fine-mapped SNPs that we identified (Supplementary Table 22) may aid efforts to link SNPs to genes[42–44]. Fourth, SNPs that were fine-mapped for multiple genetically uncorrelated traits may shed light on shared biological pathways[58]. Fifth, sets of SNPs causally explaining 50% of common SNP heritability can potentially be used for gene and pathway enrichment analysis[59,60]. Finally, PolyFun can incorporate additional functional annotations at negligible additional computational cost, motivating further efforts to identify conditionally informative annotations.

Our work has several limitations. First, we recommend applying PolyFun using summary LD information from the same samples used to compute summary association statistics, as previously recommended for fine-mapping methods[12,30]. This information is not always available; however, we have publicly released summary LD information from the UK Biobank samples that we analyzed (see URLs), and continue to encourage future studies to publicly release summary LD information together with summary association statistics[61]. Second, subtle population stratification may lead to spurious fine-mapping results, arising from spurious association results[62]. However, our fine-mapped SNPs are concentrated in associated loci with larger estimated effects, which are relatively less likely to be spurious. Third, we did not compare PolyFun to the functionally informed fine-mapping method applied in ref. [10] (an extension of fGWAS[21]), which was not made publicly available. However, that method can only incorporate a limited number of functional annotations (e.g. <15 in ref. [10]) and uses stepwise conditional fine-mapping, which has been shown to be susceptible to spurious findings[30]. Fourth, PolyFun + SuSiE and PolyFun + FINEMAP, like other methods, were well-calibrated in simulations when using conservative false-discovery thresholds but not always well-calibrated when using exact false-discovery thresholds, demonstrating the challenges of exact calibration in fine-mapping. We thus recommend setting PIP>0.95 (resp. PIP>0.5) estimates to PIP=0.95 (resp. PIP=0.5) when interpreting empirical results. Fifth, PolyFun + SuSiE assumes 10 causal SNPs per locus (Table 1). This choice has been shown to have minimal impact on SuSiE results[22], but it may still be advantageous to assess the number of causal SNPs per locus in a data-driven manner. Sixth, PolyFun (and SuSiE) were designed for quantitative phenotypes but can also be applied to binary phenotypes;

bioRxiv preprint doi: https://doi.org/10.1101/807792; this version posted October 29, 2019. The copyright holder for this preprint (which was not certified by peer review) is the author/funder, who has granted bioRxiv a license to display the preprint in perpetuity. It is made available under aCC-BY 4.0 International license.

alternative methods designed for binary phenotypes may further increase power. Seventh, we restricted our analyses to MAF>0.001 SNPs, because SNPs with lower MAFs are often not well-imputed[63]. Future studies with whole genome sequencing data could potentially fine-map MAF≤0.001 SNPs, but the performance of PolyFun + SuSiE on sequencing data has not been investigated. Eighth, we performed fine-mapping using 3Mb windows, but in rare cases causal SNPs might be in LD with associated SNPs that are outside these windows. Ninth, application of PolyLoc requires analyzing samples distinct from the samples analyzed by PolyFun to avoid winner's curse. Researchers with access to individual-level genetic data can partition the samples as we have done (we recommend using approximately 75% of the data for fine-mapping and 25% for polygenic localization). A potential alternative is to apply methods to alleviate bias due to winner's curse[64,65]. We emphasize that not correcting for winner's curse can lead to extremely biased estimates (Supplementary Table 28). Tenth, PolyLoc provides an upper bound on the proportion of SNPs causally explaining a given proportion of SNP-heritability, and is thus conservative. Finally, multi-ethnic fine-mapping[66] and incorporation of tissue-specific functional annotations[9,13,15,17] may further increase fine-mapping power. Incorporating these into our fine-mapping framework is an avenue for future work.

bioRxiv preprint doi: https://doi.org/10.1101/807792; this version posted October 29, 2019. The copyright holder for this preprint (which was not certified by peer review) is the author/funder, who has granted bioRxiv a license to display the preprint in perpetuity. It is made available under aCC-BY 4.0 International license.

Methods

PolyFun fine-mapping method

PolyFun performs functionally-informed fine-mapping by first estimating prior causal probabilities for all SNPs and then applying fine-mapping methods such as SuSiE[22] or FINEMAP[23,24] with these prior causal probabilities. Here we describe estimation of the prior causal probabilities.

We model standardized phenotypes y using the linear model $y = \sum_i x_i \beta_i + \epsilon$, where x_i denotes standardized SNP genotypes, β_i denotes effect size, and ϵ is a residual term. We use a point-normal model for β_i:

$$\beta_i | \boldsymbol{a}_i \sim \begin{cases} \mathcal{N}(0, \mathrm{var}[\beta_i | \beta_i \neq 0]) & \text{with probability } \mathrm{P}(\beta_i \neq 0 | \boldsymbol{a}_i) \\ 0 & \text{otherwise} \end{cases},$$

where $\boldsymbol{a}_i$ are the functional annotations of SNP i, $P(\beta_i \neq 0 | \boldsymbol{a}_i)$ is its prior causal probability, and $\mathrm{var}[\beta_i | \beta_i \neq 0]$ is its causal variance, which we assume is independent of $\boldsymbol{a}_i$. This assumption is motivated by our recent work showing that functional enrichment is primarily due to differences in polygenicity rather than differences in effect-size magnitude, which is constrained by negative selection[29].

The key quantity that PolyFun uses to estimate prior causal probabilities is the per-SNP heritability of SNP i, $\mathrm{var}[\beta_i | \boldsymbol{a}_i]$ (we refer to this quantity as per-SNP heritability because the total SNP-heritability $\mathrm{var}[\sum_i x_i \beta_i \,|\boldsymbol{a}]$ is equal to $\sum_i \mathrm{var}[\beta_i | \boldsymbol{a}_i]$, assuming that causal SNP effects have zero mean and are uncorrelated with other SNP effects and with other SNPs conditional on $\boldsymbol{a}$). PolyFun relates the prior causal probability $\mathrm{P}(\beta_i \neq 0 | \boldsymbol{a}_i)$ to the per-SNP heritability $\mathrm{var}[\beta_i | \boldsymbol{a}_i]$ via the law of total variance:

$$\mathrm{P}(\beta_i \neq 0 | \boldsymbol{a}_i) = \frac{\mathrm{var}[\beta_i | \boldsymbol{a}_i]}{\mathrm{var}[\beta_i | \beta_i \neq 0]}. \qquad (2)$$

Equation 1 in the main text follows since $\mathrm{P}(\beta_i \neq 0 | \boldsymbol{a}_i)$ is proportional to $\mathrm{var}[\beta_i | \boldsymbol{a}_i]$ with the proportionality factor $1/\mathrm{var}[\beta_i | \beta_i \neq 0]$.

To derive Equation 2 we define the causality indicator $c_i = \mathbb{I}[\beta_i \neq 0 | \boldsymbol{a}_i]$ and apply the law of total variance to $\mathrm{var}[\beta_i | \boldsymbol{a}_i]$:

$$\begin{aligned} \mathrm{var}[\beta_i | \boldsymbol{a}_i] &= \mathrm{E}_{c_i}\big[\mathrm{var}[\beta_i | \boldsymbol{a}_i, c_i]\big] + \mathrm{var}_{c_i}\big[\mathrm{E}[\beta_i | \boldsymbol{a}_i, c_i]\big] \\ &= \mathrm{E}_{c_i}\big[\mathrm{var}[\beta_i | \boldsymbol{a}_i, c_i]\big] + \mathrm{var}_{c_i}[0] \\ &= \mathrm{P}(c_i = 0) \cdot 0 + \mathrm{P}(c_i = 1)\mathrm{var}[\beta_i | \boldsymbol{a}_i, c_i = 1] \\ &= \mathrm{P}(\beta_i \neq 0 | \boldsymbol{a}_i)\mathrm{var}[\beta_i | \boldsymbol{a}_i, \beta_i \neq 0] \\ &= \mathrm{P}(\beta_i \neq 0 | \boldsymbol{a}_i)\mathrm{var}[\beta_i | \beta_i \neq 0]. \end{aligned}$$

The last equality holds because we assume that the causal effect size variance is independent of functional annotations, as explained above.

PolyFun avoids directly estimating the proportionality factor $1/\mathrm{var}[\beta_i | \beta_i \neq 0]$ by constraining the prior causal probabilities $\mathrm{P}(\beta_i \neq 0 | \boldsymbol{a}_i)$ in each tested locus to sum to 1.0. This constraints implies that each locus is a-priori expected to harbor one causal SNPs, consistent with previous fine-mapping methods[5,6,23] (we note that this constraint is ignored by PolyFun + SuSiE, because it is invariant to scaling of prior causal probabilities). Hence, the main challenge is estimating the per-SNP heritabilities $\mathrm{var}[\beta_i | \boldsymbol{a}_i]$.

bioRxiv preprint doi: https://doi.org/10.1101/807792; this version posted October 29, 2019. The copyright holder for this preprint (which was not certified by peer review) is the author/funder, who has granted bioRxiv a license to display the preprint in perpetuity. It is made available under aCC-BY 4.0 International license.

To estimate $\mathrm{var}[\beta_i|\boldsymbol{a}_i]$, PolyFun incorporates a regularized extension of S-LDSC with the baseline-LF model[17,25–27], which we extend to a new version 2.2.UKB (Supplementary Table 1, URLs, see below). S-LDSC uses the linear model $\mathrm{var}[\beta_i|\boldsymbol{a}_i] = \sum_c \tau^c a_i^c$ and jointly estimates all τ^c parameters by minimizing the term $\sum_\mathrm{i}\left(\chi_i^2 - n\sum_c \tau^c l(i,c) - nb - 1\right)^2$, where c are functional annotations, τ^c is the coefficient of annotation c, χ_i^2 is the χ^2 statistic of SNP i, n is the sample size, b measures the contribution of confounding biases, and $l(i,c) = \sum_j r_{ij}^2\, a_j^c$.

While S-LDSC produces robust estimates of functional enrichment, it has two limitations in estimating $\mathrm{var}[\beta_i|\boldsymbol{a}_i]$: (i) these estimates can have large standard errors in the presence of many annotations, and (ii) the model may not be robust to model misspecification. To address the first limitation, PolyFun incorporates an L2-regularized extension of S-LDSC. To address the second limitation, PolyFun employs special procedures to ensure robustness to model misspecification. The key idea is to approximate arbitrary complex functional forms of $\mathrm{var}[\beta_i|\boldsymbol{a}_i]$ via a piecewise-constant function. To do this, PolyFun partitions SNPs with similar estimated values of $\mathrm{var}[\beta_i|\boldsymbol{a}_i]$ (estimated via a possibly misspecified model) into non-overlapping bins; estimates the SNP-heritability causally explained by each bin b; and specifies $\mathrm{var}[\beta_i|\boldsymbol{a}_i]$ for SNPs in bin b as the SNP-heritability causally explained by bin b divided by the number of SNPs in bin b. PolyFun avoids winner's curse by using different data for partitioning SNPs and for per-bin heritability estimation.

In detail, PolyFun robustly specifies prior causal probabilities for all SNPs on a target locus on a corresponding odd (resp. even) target chromosome via the following procedure:

1. Estimate annotation coefficients $\hat{\tau}_{\mathrm{even}}^c$ and intercepts $\hat{b}_{\mathrm{even}}$ using only SNPs in even chromosomes via an L2-regularied extension of S-LDSC that minimizes $\sum_\mathrm{i}\left(\chi_i^2 - n\sum_c \hat{\tau}_{\mathrm{even}}^c l(i,c) - n\hat{b}_{\mathrm{even}} - 1\right)^2 + \lambda\sum_c(\hat{\tau}_{\mathrm{even}}^c)^2$ (resp. using $\hat{\tau}_{\mathrm{odd}}^c$ and $\hat{b}_{\mathrm{odd}}$). We select the regularization strength λ from a geometrically-spaced grid of 100 values ranging from 10^{-8} to 100, selecting the one that minimizes the average out-of-chromosome error $\sum_r\sum_{\mathrm{i}\in\mathrm{r}}\left(\chi_i^2 - n\sum_c \hat{\tau}_{\mathrm{even}\backslash\mathrm{r}}^c l(i,c) - n\hat{b}_{\mathrm{even}\backslash\mathrm{r}} - 1\right)^2$, where r iterates over even (resp. even) chromosomes, and $\hat{\tau}_{\mathrm{even}\backslash\mathrm{r}}^c$, $\hat{b}_{\mathrm{even}\backslash\mathrm{r}}$ are the S-LDSC τ and b estimates, respectively, when applied to all SNPs on even chromosomes except for chromosome r (resp. for odd chromosomes).
2. Compute per-SNP heritabilities $\widehat{\mathrm{var}}[\beta_i|\boldsymbol{a}_i] = \sum_c \hat{\tau}_{\mathrm{even}}^c a_i^c$ for each SNP i in an odd chromosome (resp. $\sum_c \hat{\tau}_{\mathrm{odd}}^c a_i^c$).
3. Partition all SNPs into 20 bins with similar values of $\widehat{\mathrm{var}}[\beta_i|\boldsymbol{a}_i]$ using the Ckmedian.1d.dp method[67]. This method partitions SNPs into 20 maximally homogenous bins such that the average distance of $\widehat{\mathrm{var}}[\beta_i|\boldsymbol{a}_i]$ to the median $\widehat{\mathrm{var}}[\beta_i|\boldsymbol{a}_i]$ of the bin of SNP i is minimized. We emphasize that even though this step uses functional annotations data of the target chromosome it does not use the summary statistics of SNPs in the target chromosome, which ensures robustness to winner's curse.
4. Apply S-LDSC with non-negativity constraints to estimate per-SNP heritabilities in each of the 20 bins of all SNPs in odd (resp. even) chromosomes except for the target chromosome r (to avoid using the same data that will be used in fine-mapping), denoted $\hat{\sigma}_{r,1}^2, \ldots, \hat{\sigma}_{r,20}^2$. Afterwards, regularize the estimates by setting all values smaller than $q \cdot \max_\mathrm{b}(\hat{\sigma}_{r,b}^2)$ to $q \cdot \max_\mathrm{b}(\hat{\sigma}_{r,b}^2)$, using $q = 1/100$ by default, and rescaling the $\hat{\sigma}_{r,b}^2$ estimates to have the same sum (over all genome-wide SNPs) as before. The regularization prevents SNPs from a having a zero per-SNP probability, which would exclude them from fine-mapping. We did not apply L2-regularization in this step because we require approximately

bioRxiv preprint doi: https://doi.org/10.1101/807792; this version posted October 29, 2019. The copyright holder for this preprint (which was not certified by peer review) is the author/funder, who has granted bioRxiv a license to display the preprint in perpetuity. It is made available under aCC-BY 4.0 International license.

unbiased estimates, and because standard errors are relatively small in the presence of a small number of non-overlapping annotations.

5. Specify a prior causal probability proportional to $\hat{\sigma}^2_{r,b}$ to each SNP that is in bin b and that resides in a target locus in chromosome r, such that the prior causal probabilities in the target locus sum to one.

PolyFun uses version 2.2.UKB of the baseline-LF model, which differs from the original baseline-LF model[26] by including MAF≥0.001 SNPs and several new annotations, and omitting annotations that could not be easily extended to account for MAF<0.005 SNPs (Supplementary Table 1). Briefly, we use 187 overlapping functional annotations, including 10 common MAF bins (MAF≥0.05); 10 low-frequency MAF bins (0.05>MAF≥0.001); 6 LD-related annotations for common SNPs (levels of LD, predicted allele age, recombination rate, nucleotide diversity, background selection statistic, CpG content); 5 LD-related annotations for low-frequency SNPs; 40 binary functional annotations for common SNPs; 7 continuous functional annotations for common SNPs; 40 binary functional annotations for low-frequency SNPs; 3 continuous functional annotations for low-frequency SNPs; and 66 annotations constructed via windows around other annotations[17]. We did not include a base annotation that includes all SNPs, because such an annotation is linearly dependent on all the MAF bins when S-LDSC uses the same set of SNPs to compute LD-scores and to estimate annotation coefficients.

Fine-mapping simulations

We simulated summary statistics for 18,212,157 genotyped and imputed MAF≥0.001 autosomal SNPs with INFO score≥0.6 (including short indels, excluding three long-range LD regions; see below), using N=337,491 unrelated British-ancestry individuals from UK Biobank release 3. In most simulations we computed an effect variance β_i for every SNP i with annotations $\boldsymbol{a}_i$ using the baseline-LF (version 2.2.UKB) model, $\mathrm{var}[\beta_i|\boldsymbol{a}_i] = \sum_c \tau^c a_i^c$, where c are annotations and τ^c estimates are taken from a fixed-effects meta-analysis of 16 well-powered genetically uncorrelated ($|r_g|$<0.2) UK Biobank traits (age of menarche, BMI, balding, bone mineral density, eosinophil count, FEV1/FVC ratio, forced vital capacity, hair color, height, platelet count, red blood cell distribution width, red blood cell count, systolic blood pressure, tanning, waist-hip ratio adjusted for BMI, white blood count), scaled such that $\sum_i \mathrm{var}[\beta_i|\boldsymbol{a}_i]$ is the same across all traits (Supplementary Table 3). In some simulations we generated values of $\mathrm{var}[\beta_i|\boldsymbol{a}_i]$ under alternative functional architectures to evaluate the robustness of PolyFun to modeling misspecification (see below). Each SNP was set to be causal with probability proportional to $\mathrm{var}[\beta_i|\boldsymbol{a}_i]$, such that the average causal probability was equal to the desired proportion of causal SNPs.

To facilitate the simulations we generated summary statistics directly, without first generating phenotypic values. This is mathematically equivalent to direct simulations but is substantially faster and allows modifying the residual variance for any desired sample size n. Specifically, we sampled a vector of marginal effect sizes $\boldsymbol{\alpha}$ in each locus from $\mathcal{N}(\boldsymbol{R\beta}, \boldsymbol{R} \cdot \sigma_e^2/n)$ where $\boldsymbol{R}$ is a matrix of summary LD information (computed via LDstore[30]), $\boldsymbol{\beta}$ are effect sizes sampled iid from $\mathcal{N}(0, \sigma_c^2)$ for causal SNPs (and set to 0 for non-causal SNPs), and $\sigma_e^2 = 1 - \boldsymbol{\beta}^T\boldsymbol{R\beta}$ is the phenotypic variance not causally explained by SNPs in the locus[23,68] (see below). The causal variance σ_c^2 was set to h_g^2/m_c where h_g^2 is the desired SNP heritability and m_c is the expected number of causal SNPs. We note that modifying n implies that $\boldsymbol{R}$ represents summary LD information from the population rather than from the sample.

bioRxiv preprint doi: https://doi.org/10.1101/807792; this version posted October 29, 2019. The copyright holder for this preprint (which was not certified by peer review) is the author/funder, who has granted bioRxiv a license to display the preprint in perpetuity. It is made available under aCC-BY 4.0 International license.

We used the above procedure in two ways. First, we generated 100 sets of summary statistics in each of 10 3Mb loci in chromosome 1 for the fine-mapping experiments (selected by sorting all loci according to number of SNPs and selecting a uniformly-spaced set of loci spanning the two loci with the smallest and largest number of SNPs; Supplementary Table 2). We set h_g^2 to the desired locus heritability and m_c to the desired number of causal SNPs in the locus, for a total of 1000 simulations (for simulations based on SuSiE and FINEMAP with default parameters) or 100 simulations (for all other simulations, due to computational cost) per unique combination of settings. Second, we generated 5 sets of genome-wide summary statistics for functional enrichment estimation, setting h_g^2 to the desired genome-wide SNP-heritability and m_c to the expected genome-wide number of causal SNPs. In the genome-wide simulations we generated a summary statistic α_i for each SNP based on the locus whose center was closest to the SNP among 2,763 overlapping 3Mb loci spanning all autosomal chromosomes (with a 1Mb spacing between the start points of consecutive loci and excluding three long-range LD regions: chr6 25.5M-33.5M, chr8 8M-12M, chr11 46M-57M; see below). In each experiment we randomly selected one of the 5 genome-wide sets of summary statistics and used it to estimate functional enrichment.

The default parameters for the locus-specific simulations were m_c=10 and h_g^2=0.0005 (broadly consistent with empirical data; average h_g^2 of a 3Mb locus across 15 genetically uncorrelated traits=0.0003). The default parameters for the genome-wide simulations were m_c=91,700 (implying a proportion 0.5% of causal SNPs) and h_g^2=0.25 (consistent with real data results; Supplementary Table 11).

The most challenging aspect of the simulations is sampling vectors from $\mathcal{N}(\boldsymbol{R\beta}, \boldsymbol{R} \cdot \sigma_e^2/n)$, as it is both computationally intensive and technically complex due to singularity of $\boldsymbol{R}$. To circumvent these challenges we sampled 100 $\boldsymbol{\alpha}_e$ vector from $N(\boldsymbol{0}, \boldsymbol{R})$ for each locus and stored them for future use. Afterwards, we generated summary statistics in each simulation via $\boldsymbol{\alpha} = \boldsymbol{R\beta} + \boldsymbol{\alpha}_e \cdot \sigma_e^2/n$, randomly choosing one of the 100 $\boldsymbol{\alpha}_e$ vectors. Because $\boldsymbol{R}$ was typically singular, we sampled $\boldsymbol{\alpha}_e$ approximately by (1) taking a random maximal subset of SNPs such that no pair of SNPs has $|r|$>0.99, using the maximal_independent_set procedure in the NetworkX package[69], and constructing the corresponding submatrix $\boldsymbol{R}_s$; (2) Finding the minimum value of γ such that $(1-\gamma)\boldsymbol{R}_s + \gamma\boldsymbol{I}$ has a minimal eigenvalue >0.0001; (3) sampling $\boldsymbol{\alpha}_{e,s}$ from $N(\boldsymbol{0}, (1-\gamma)\boldsymbol{R}_s + \gamma\boldsymbol{I})$; (4) sampling a value α_e^i for each SNP i that was omitted in step 1 from a normal distribution conditional on $\alpha_{e,s}^j$ of the non-omitted SNP j having the strongest LD with SNP i; and (5) constructing $\boldsymbol{\alpha}_e$ by combining $\boldsymbol{\alpha}_{e,s}$ and all values of α_e^i.

After generating summary statistics, we first estimated prior causal probabilities for all SNPs as described in the PolyFun fine-mapping method subsection. We ran S-LDSC using LD scores computed from the summary LD information used to generate summary statistics (based on imputed SNP dosages rather than sequenced genotypes as in previous publications that used S-LDSC[25–27], assigning to each SNP the LD score computed in the locus in which it was most central) to obtain sufficient coverage of low-frequency SNPs, which are underrepresented in small external reference panels.

We performed fine-mapping in each of the 10 selected 3Mb loci on chromosome 1 using methods based on SuSiE[22], FINEMAP[23,24], CAVIARBF[20] and fastPAINTOR[19]. Following previous literature[12,30] all methods used summary LD information computed via LDstore[30] from the genotypes of the same 337,491 individuals used to generate summary statistics.

For fastPAINTOR-, fastPAINTOR, SuSiE, and PolyFun + SuSiE, we specified a causal effect size variance using an estimator that we developed based on a modified version of HESS[70] rather than using the estimator

bioRxiv preprint doi: https://doi.org/10.1101/807792; this version posted October 29, 2019. The copyright holder for this preprint (which was not certified by peer review) is the author/funder, who has granted bioRxiv a license to display the preprint in perpetuity. It is made available under aCC-BY 4.0 International license.

implemented in these methods, because it improved false discovery rate and power in most simulation settings (Supplementary Table 4). Briefly, HESS estimates regional SNP-heritability via $\boldsymbol{\alpha}\boldsymbol{R}^{-1}\boldsymbol{\alpha} - m/n$, where $\boldsymbol{\alpha}$ is a vector of marginal effect size estimates for m standardized SNPs, $\boldsymbol{R}$ is a matrix of summary LD information, and n is the sample size. We regularized this estimator (using summary LD information computed directly from the genotypes of the individuals used to generate summary statistics) by (1) excluding SNPs having α_i^2<0.00005 (i.e., having a negligible contribution to the estimator); and (2) selecting a random maximal subset of the remaining SNPs such that no pair of SNPs has $|r|$>0.99. We averaged this estimate across 100 different estimates per locus, each time selecting a different random subset via the maximal_independent_set procedure in the NetworkX package[69]. We then estimated the causal effect size variance as the HESS estimator divided by the assumed number of causal SNPs (using a value of 10 by default in this work). The division assumes that the correlation between causal SNPs is zero in expectation.

We now describe the parameters provided to each fine-mapping method.

We ran SuSiE 0.7.1.0487 with default values for all parameters except the following: (1) We used 10 causal SNPs per locus; and (2) we estimated a per-locus causal effect size variance (the scaled_prior_variance parameter) via our modified HESS approach. We specified prior causal probabilities via the prior_weights parameter. We modified the SuSiE source code to avoid performing the LD matrix diagnostics (positive-definiteness and symmetry) because they greatly increased memory consumption.

We ran FINEMAP 1.3.1.b (a new version of FINEMAP that we introduce here that incorporates prior causal probabilities) with a maximum of 10 causal SNPs per locus and with default settings for all other parameters. We specified prior causal probabilities via the –prior-snps argument.

We ran CAVIARBF 0.2.1 with an AIC-based parameter selection, using ridge regression with regularization parameter λ selected from {2^{-10}, 2^{-5}, $2^{-2.5}$, 2^{0}, $2^{2.5}$, 2^{5}, 100, 1000, 10000, 100000}, with a single locus and with up to either 1 or 2 causal SNPs per locus, owing to computational limitations.

We ran fastPAINTOR 3.1 in MCMC mode. We specified a per-locus causal effect size variance (specified via the -variance argument) using our modified HESS approach (as in PolyFun + SuSiE). We avoided truncation of the LD matrix (using prop_ld_eigenvalues=1.0) because we used in-sample summary LD information. As fastPAINTOR is generally not designed to work with >10 annotations[18,19] (and was too slow in our simulations to estimate the significance of each annotation and include only conditionally significant annotations as done in ref. [18]), we selected a subset of 10 highly informative annotations by (1) scoring each annotation based on its average contribution to effect variance $|a_i^c \tau^c|$ across all SNPs, using the true τ^c of the generative model; (2) iteratively selecting top-ranked annotations such that no annotation has correlation >0.3 (in absolute value) with a previously selected annotation, until selecting 10 annotations. We determined that 10 annotations yielded approximately optimal power while maintaining correct calibration (Supplementary Table 4).

For each PIP threshold, we conservatively estimated false discovery rates by setting all PIPs greater than the threshold to the threshold, yielding a uniform false-discovery threshold. This differs from exact false-discovery thresholds, defined as one minus the average PIP across all SNPs with PIP greater than the PIP threshold (e.g., if all SNPs with PIP>0.95 have PIP=1 then the expected false-discovery rate is 0% rather than 5%). We evaluated the results with respect to exact false-discovery thresholds in secondary analyses.

bioRxiv preprint doi: https://doi.org/10.1101/807792; this version posted October 29, 2019. The copyright holder for this preprint (which was not certified by peer review) is the author/funder, who has granted bioRxiv a license to display the preprint in perpetuity. It is made available under aCC-BY 4.0 International license.

In a subset of the simulations we evaluated two alternative functional architectures: (1) A multiplicative functional architecture defined by $\mathrm{var}[\beta_i|\boldsymbol{a}_i] = \exp(\sum_c \gamma^c a_i^c) = \prod_c \exp(\gamma^c a_i^c)$, where γ^c is the coefficient of annotation c; and (2) a sub-additive functional architecture defined by $\mathrm{var}[\beta_i|\boldsymbol{a}_i] = \max\{a_i^c \omega_c\}$, where ω_c is the coefficient of annotation c. To obtain realistic functional architectures, we fitted the coefficients of these two models to obtain a distribution of $\mathrm{var}[\beta_i|\boldsymbol{a}_i]$ that is roughly similar to the distribution obtained under the standard S-LDSC with the baseline-LF model (with meta-analyzed linear annotation coefficients τ^c; see above). In the multiplicative functional architecture, we fitted γ^c by approximately minimizing the mean squared distance between $\prod_c \exp(\gamma^c a_i^c)$ and $\sum_c \tau^c a_i^c$ (via a linear regression with a_i^c as explanatory variables and $\log \sum_c \tau^c a_i^c$ as the outcome, setting all estimates smaller than the median of the non-negative values of $\sum_c \tau^c a_i^c$ to the median to prevent the regression from being dominated by SNPs with low values of $\sum_c \tau^c a_i^c$). In the sub-additive functional architecture, we partitioned annotations into six groups (non-synonymous, coding, conserved, promoter or enhancer, histone marks, repressed, others) and associated all annotations in each group with the same coefficient ω_c, such that the mean squared distance between $\max\{a_i^c \omega_c\}$ and $\sum_c \tau^c a_i^c$ is minimized.

Functionally informed fine-mapping of 47 complex traits in the UK Biobank

We applied SuSiE and PolyFun + SuSiE to fine-map 47 traits in the UK Biobank, including 31 traits analyzed in refs. [34,35], 9 blood cell traits analyzed in ref. [12], and 7 recently released metabolic traits (average *N*=317K; Supplementary Table 5), using the same data and the same parameter settings described in the Fine-mapping simulations section. We performed basic QC on each trait as described in our previous publications[34,35]. Specifically, we removed outliers outside the reasonable range for each quantitative trait, and quantile normalizing within sex strata after correcting for covariates for non-binary traits with non-normal distributions. We computed summary statistics with BOLT-LMM v2.3.3[35] adjusting for sex, age and age squared, assessment center, genotyping platform, and the top 20 principal components (computed as described in ref. [35]), and dilution factor for biochemical traits. As the non-infinitesimal version of BOLT-LMM does not estimate effect sizes, we computed z-scores for fine-mapping by taking the square root of the BOLT-LMM χ^2 statistics and multiplying them by the sign of the effect estimate from the infinitesimal version of BOLT-LMM.

We partitioned each autosomal chromosome into 2,763 overlapping 3Mb-long loci with a 1Mb spacing between the start points of consecutive loci. We computed a PIP for each SNP based on the locus whose center was closest to the SNP (excluding SNPs >1Mb away from the closest center and loci wherein all SNPs had squared marginal effect sizes smaller than 0.00005). We excluded the MHC region (chr6 25.5M-33.5M) and two other long-range LD regions (chr8 8M-12M, chr11 46M-57M)[71] from all analyses, following our observations that both methods tend to produce spurious results in these regions, finding many PIP=1 SNPs across many traits regardless of their BOLT-LMM p-values. We verified that other previously reported long-range LD regions[71] do not harbor a disproportionate number of PIP>0.95 SNPs. We specified per-locus causal effect variances for SuSiE and PolyFun + SuSiE via our modified HESS approach. For all S-LDSC and fine-mapping analyses we specified a sample size corresponding to the BOLT-LMM effective sample size[35] (given by the true sample size multiplied by the median ratio between χ^2 statistics of BOLT-LMM and linear regression across SNPs with BOLT-LMM χ^2>30).

bioRxiv preprint doi: https://doi.org/10.1101/807792; this version posted October 29, 2019. The copyright holder for this preprint (which was not certified by peer review) is the author/funder, who has granted bioRxiv a license to display the preprint in perpetuity. It is made available under aCC-BY 4.0 International license.

All S-LDSC analyses used LD scores computed from in-sample summary LD information (based on imputed SNP dosages rather than sequenced genotypes as in previous publications[25–27], assigning to each SNP the LD score computed in the locus in which it was most central) because they provide better coverage of low-frequency SNPs and are consistent with the fine-mapping analyses. We computed genetic correlations with LDSC, using the same summary statistics used for fine-mapping and restricting the analysis to common SNPs.

We selected a subset of 15 genetically uncorrelated traits by ranking all traits according to the number of PolyFun + SuSiE PIP>0.95 SNPs and greedily selecting top-ranked traits such that no selected trait has $|r_g|$>0.2 with a previously selected trait, excluding traits having either (1) h_g^2 estimates <0.05 in either the PolyFun dataset (N=337K) or in the PolyLoc dataset (N=122K) (see h_g^2 estimation description below); or (2) traits with an effective sample size <100K in the N=337K dataset (using 4/(1/#cases + 1/#controls) for binary traits).

We estimated h_g^2 tagged by PIP>0.95 SNPs and by lead GWAS SNPs via a multivariate linear regression. We regressed all the covariates used in BOLT-LMM out of the phenotypes, performed multivariate linear regression on the residuals (using all PIP>0.95 SNPs as explanatory variables) and reported the adjusted R^2 as the h_g^2 tagged by these SNPs. We verified that the results remained nearly identical regardless of whether we excluded related individuals (Supplementary Table 11). We estimated MAF>0.001 SNP-heritability for trait selection and for Figure 3b by running S-LDSC with all the baseline-LF annotations. We overrode the automatic removal of very large effect SNPs employed by S-LDSC for hair color, because this removal led to h_g^2 estimates that were smaller than the linear regression-based estimates, due to the large proportion of SNP-heritability originating from very large-effect SNPs.

We defined top annotations for Table 2, Figure 5 and Supplementary Tables 12-13 by first ranking all annotations according to their functional enrichment among PIP>0.95 SNPs (as in Figure 6; see below), and associating each SNP with its top ranked annotation, using meta-analyzed enrichment.

We selected a subset of genetically uncorrelated traits for each SNP (used in Figure 4, Table 2 and Supplementary Table 12), aiming to select traits from a diverse a set of groups as possible (anthropometric, lipids/metabolic, blood, cardiovascular/metabolic disease, other; Figure 4, Supplementary Table 5). To this aim, we iterated over trait groups cyclically. For each group containing ≥1 unselected traits with PIP>0.95 for the analyzed SNP, we selected the trait having the smallest average $|r_g|$ with unselected traits from other groups (if there remained any) or from all remaining traits (otherwise), selecting among all traits having $|r_g|$<0.2 with previously selected traits, until no more eligible traits remained. We plotted the ideogram in Figure 4 with the PhenoGram[72] software.

We computed enrichment of functional annotations among fine-mapped SNPs (Figure 6) as the ratio between the proportion of common SNPs with PIP above a given threshold having a specific annotation and the proportion of common SNPs having the annotation. We excluded continuous annotations and annotations constructed via windows around other annotations, and merged concordant annotations for common and low-frequency variants. We computed P-values using Fisher's exact test (meta-analyzed across traits via Fisher's method). We computed standard errors by (1) computing the standard error s of the log of the enrichment via the standard formula for the standard error of relative risk (exploiting the fact that enrichment and relative risk are both ratios of proportions); and (2) computing the standard

bioRxiv preprint doi: https://doi.org/10.1101/807792; this version posted October 29, 2019. The copyright holder for this preprint (which was not certified by peer review) is the author/funder, who has granted bioRxiv a license to display the preprint in perpetuity. It is made available under aCC-BY 4.0 International license.

error of the enrichment via $\sqrt{r^2(e^{s^2}-1)}$ (i.e., the standard deviation of the exponent of a normal random variable), where r is the original enrichment estimate (meta-analyzed across traits using a fixed-effects meta-analysis). We excluded traits having <10 PIP>0.95 SNPs from the meta-analysis. The annotations shown in Figure 6 are non-synonymous, Conserved_LindbladToh (denoted Conserved), Human_Promoter_Villar_ExAC (denoted Promoter-ExAC), H3K4me3_Trynka (denoted H3K4me3), and Repressed_Hoffman (denoted Repressed).

To compare our fine-mapping results with those of refs.[7,12], we restricted the comparison to SNPs that were not excluded from our fine-mapping procedure (SNPs having MAF≥0.001 in the UK Biobank *N*=337K dataset, INFO score≥0.6, distance <1Mb away from the closest locus center, and not residing in one of the excluded long-range LD regions). When the same SNP had multiple reported PIPs in ref. [12], we used the entry with the larger PIP. We caution that the comparison with ref. [12] is not a replication analysis because the datasets of ref. [12] and of PolyFun + SuSiE are correlated.

We selected traits for down-sampling analysis (analyzing *N*=107K individuals) as the set of traits having (1) the largest number of 3Mb significant loci harboring a genome-wide significant SNP; (2) >10 PIP>0.95 SNPs in the SuSiE *N*=107K analysis; and (3) $|r_g|$<0.2 with another selected trait.

Polygenic localization

Polygenic localization aims to identify a minimal set of SNPs causally explaining a given proportion of common SNP heritability. To formally define polygenic localization, we first define expected common SNP heritability under a fixed effects model with no autocorrelation. We assume the linear model $y = \sum_{i=1}^{m} x_i\beta_i + \epsilon$, where y is a phenotype, x_i is a standardized common SNP with effect β_i, m is the number of common SNPs and ϵ is a residual term. We define the expected common SNP heritability $\mathrm{E}h^2$ as follows:

$$\mathrm{E}h^2 = \sum_{i=1}^{m} \beta_i^2 .$$

This definition stems from the fixed effects SNP-heritability $\mathrm{var}[\sum_i x_i\beta_i \mid \boldsymbol{\beta}] = \sum_i \beta_i^2 + 2\sum_{\mathrm{i,j}} r_{ij}\beta_i\beta_j$, where we assumed standardized genotypes, r_{ij} is the LD between SNPs i, j, and the second term on the right hand size is zero in expectation, assuming no autocorrelation. We next define the expected common SNP heritability of a subset $\boldsymbol{S}$ of SNPs by:

$$\mathrm{E}h_{\boldsymbol{S}}^2 = \sum_{i\in\boldsymbol{S}} \beta_i^2 .$$

We define M_p^*, the smallest set of common SNPs causally explaining proportion p of expected common SNP heritability, as the cardinality of the smallest set $\boldsymbol{S}$ such that $\mathrm{E}h_{\boldsymbol{S}}^2/\mathrm{E}h^2 \geq p$. An equivalent definition is the smallest integer k such that

$$\frac{\sum_{i\in\{s_1,\ldots,s_k\}} \beta_i^2}{\sum_{i=1}^{m} \beta_i^2} \geq p,$$

where s_j denotes a ranking of β_i^2 such that $\beta_{s_1}^2 \geq \beta_{s_2}^2 \geq \cdots \geq \beta_{s_m}^2$. We analogously define M_p with respect to a given (possibly non-optimal) ranking of SNPs s' as the smallest integer k' such that $\sum_{i\in\{s'_1,\ldots,s'_{k'}\}} \beta_i^2 \,/\, \sum_{i=1}^{m} \beta_i^2 \geq p$. We note that $M_p \geq M_p^*$ by construction.

bioRxiv preprint doi: https://doi.org/10.1101/807792; this version posted October 29, 2019. The copyright holder for this preprint (which was not certified by peer review) is the author/funder, who has granted bioRxiv a license to display the preprint in perpetuity. It is made available under aCC-BY 4.0 International license.

Unfortunately, β_i^2 is unknown in practice. Polygenic localization therefore estimates an upper-bound of M_p^* non-parametrically, by estimating M_p with respect to a ranking of SNPs based on PolyFun + SuSiE β_i^2 posterior mean estimates, using a random effects model. We first provide a brief conceptual description of PolyLoc and then describe it in detail below. Briefly, PolyLoc proceeds by (1) partitioning SNPs with similar β_i^2 posterior mean estimates (using PolyFun + SuSiE estimates) into bins; (2) treating β_i as a zero-mean random variable and jointly estimating $\mathrm{var}[\beta_i]$ in every bin using S-LDSC; and (3) finding the smallest integer k such that $\sum_{i\in\{\hat{s}_1,\ldots,\hat{s}_k\}}\mathrm{var}[\beta_i] \,/\, \sum_{i=1}^{m}\mathrm{var}[\beta_i] \geq p$, where $\hat{s}_j$ denotes the original ranking of β_i^2 posterior mean estimates from PolyFun + SuSiE. The use of $\mathrm{var}[\beta_i] = E\left[\beta_i^2\right] - E[\beta_i]^2$ instead of β_i^2 uses the assumption that β_i has zero mean in each bin. The partitioning into bins in step 1 induces a piecewise-linear approximation of the function $f(k) = \sum_{i\in\{s_1,\ldots,s_k\}}\beta_i^2 \,/\, \sum_{i=1}^{m}\beta_i^2$. We use different datasets to estimate β_i^2 posterior means and to estimate $\mathrm{var}[\beta_i]$ to prevent winner's curse (which occurs when performing inference based on top ranked items using the same data used for ranking). Our approach is conservative by design due to using an imperfect ranking compared to the true ranking $s_1, \ldots, s_m$. The degree of conservativeness is a function of fine-mapping power, and thus depends on factors affecting fine-mapping power such as sample size, levels of LD at causal SNPs, MAFs of causal SNPs, and trait polygenicity.

We now describe PolyLoc in detail. We used two sets of BOLT-LMM summary statistics based on different datasets: N=337,491 unrelated British-ancestry UK Biobank individuals, and N=121,768 European-ancestry UK Biobank individuals not included in the first set. PolyLoc proceeds as follows:

1. Apply median-based clustering of posterior mean estimates of β_i^2 (i.e., the sum of the squared posterior mean and of the posterior variance of β_i reported by PolyFun + SuSiE, based on the PolyFun *N*=337K dataset) into 50 bins using the Ckmedian.1d.dp method[67]. Afterwards, include all SNPs excluded from fine-mapping (e.g. SNPs in the MHC region) in the last bin, and sub-partition the last bin into 10 equally-sized MAF bins to account for MAF-based genetic architecture[26], yielding 59 bins (or 20 bins when also including non-common SNPs, yielding 69 bins). We used a larger number of bins than that used in step 3 of PolyFun because posterior mean estimates of β_i^2 follow a heavy-tailed distribution, requiring many bins to avoid placing two SNPs having effect sizes of a different order of magnitude in the same bin.
2. Jointly estimate $\mathrm{var}[\beta_i]$ of SNPs in each bin (defined as the SNP-heritability causally explained by the bin divided by the bin size) by creating an annotation for each bin and running a modified version of S-LDSC using the summary statistics from the PolyLoc *N*=122K dataset, with the following modifications: (a) use in-sample summary LD information (based on SNP dosages from imputed genotypes) to compute LD scores as in the PolyFun analyses; (b) apply non-negativity constraints to prevent negative $\mathrm{var}[\beta_i]$ estimates; and (c) retain SNPs with $\chi^2 > 80$ in the analysis. Step (c) facilitates handling of bins that predominantly consist of very large effect SNPs.
3. Rank common SNPs according to their β_i^2 posterior mean estimates from PolyFun + SuSiE (if they do not reside in MAF bins) or according to a ranking of MAF bins (otherwise). To rank MAF bins, we applied standard S-LDSC to the PolyFun dataset (N=337K in our setting) with the same bin partitioning and ranked MAF bins according to their enrichment estimates (this is needed because β_i^2 is not necessarily strongly correlated with MAF). Afterwards, compute M_p as the smallest number of top-ranked common SNPs, such that the sum of their $\mathrm{var}[\beta_i]$ estimates from step 2 is equal to proportion

bioRxiv preprint doi: https://doi.org/10.1101/807792; this version posted October 29, 2019. The copyright holder for this preprint (which was not certified by peer review) is the author/funder, who has granted bioRxiv a license to display the preprint in perpetuity. It is made available under aCC-BY 4.0 International license.

p of the sum of all $\mathrm{var}[\beta_i]$ estimates. Finally, compute standard errors of M_p via a 200-block-jackknife[73], recomputing M_p separately using the estimates of each jackknife block.

Step 2 of PolyLoc requires a set of samples (*N*=122K in our analyses) different than that used in PolyFun + SuSiE (*N*=337K in our analyses) rather than a partitioning of chromosomes to avoid winner's curse. Otherwise, PolyLoc would use the same summary statistics for both bin-partitioning and for estimating per-bin heritability (noting that this difficulty does not exist in PolyFun because PolyFun performs bin-partitions using only functional annotations, without requiring summary statistics from the target chromosome).

When computing standard errors of M_p, we excluded jackknife blocks that yielded extremely noisy estimates (yielding an M_p estimate whose distance to the median of the estimates was >25x the interquartile range of all jackknife-block estimates; typically <2 blocks per trait). Such blocks likely result from the inclusion of very large-effect SNPs in step 2 of PolyLoc.

We included all MAF>0.001 SNPs in the set of S-LDSC regression SNPs (defined in refs. [17,25,26]) regardless of whether we were interested in polygenic localization of common SNP-heritability or of MAF>0.001 SNP heritability, but did not include them in set of S-LDSC heritability SNPs (defined in refs. [17,25,26]) except in analyses of MAF>0.001 SNP heritability.

In secondary analyses, we compared PolyLoc to an alternative method that performs polygenic localization based on prior estimates of per-SNP heritability from functional annotations, rather than posterior estimates. This alternative method uses per-SNP heritability estimates and SNP bins from step 4 of PolyFun, based only on the N=337K dataset (noting that it does not suffer from winner's curse because PolyFun applies a partitioning into odd and even chromosomes).

PolyLoc will yield robust estimates of M_p if S-LDSC yields robust estimates of the SNP-heritability causally explained by each bin. Although S-LDSC has previously been shown to produce robust estimates[17,25–27], we performed extensive simulations to confirm that PolyLoc produces robust estimates of M_p. An exact simulation scheme would require first ranking all SNPs according to their PolyFun + SuSiE posterior per-SNP heritabilities, which is computationally prohibitive. To circumvent this computational challenge, we demonstrate that PolyLoc produces robust estimates of M_p with respect to several different SNP rankings. Specifically, we (1) generated causal effects for all SNPs on chromosome 1; (2) generated two independent corresponding sets of summary statistics for all SNPs on chromosome 1: A PolyFun dataset (with sampling noise based on *N*=320K individuals) and a PolyLoc dataset (with sampling noise based on *N*=122K individuals); (3) generated several different rankings of SNPs on chromosome 1 corresponding to different levels of statistical power (see below), using the PolyFun summary statistics (*N*=320K) from step 2; and (4) applied PolyLoc using the rankings from step 3, using the PolyLoc summary statistics from step 2 (*N*=122K). We generated causal effects and summary statistics in steps 1-2 as in the fine-mapping simulations (except for the restriction to chromosome 1), using LD matrices based on genotypes of 337K UK biobank individuals, such that 0.5% of the SNPs are causal and the SNPs jointly explain h_g^2=25%. We ranked SNPs in step 3 according to approximate posterior per-SNP heritabilities given by $r_i = u\beta_i^2 + (1-u)\gamma_i^2$, where β_i is the simulated causal effect of SNP i, $[\gamma_1, \dots, \gamma_m]$ is a random permutation of $[\beta_1, \dots, \beta_m]$, and $u \in \{0,0.25,0.5,0.75,1\}$ represent power levels, such that $u = 1$ indicates maximal power and $u = 0$ indicates zero power. We partitioned SNPs into 10 bins in step 4 of each simulation (rather than 50 as in the real data analyses) because we only used chromosome 1 SNPs. (We verified that the results are relatively

bioRxiv preprint doi: https://doi.org/10.1101/807792; this version posted October 29, 2019. The copyright holder for this preprint (which was not certified by peer review) is the author/funder, who has granted bioRxiv a license to display the preprint in perpetuity. It is made available under aCC-BY 4.0 International license.

insensitive to the number of bins in secondary analyses). We generated 10 simulations for each evaluated value of u, and compared the estimated and true values of M_p in each simulation (using log scale because M_p spans different orders of magnitude for different levels of p).

PolyLoc yielded slightly conservative estimates of $\log_{10} M_p$ for u>0 and slightly anti-conservative estimates for u=0 (Supplementary Table 29). For u=0.75, representing a well-powered (but not perfectly-powered) study, the average bias of $\log_{10} M_{50\%}$ was 0.007. We emphasize that we compare estimates of $\log_{10} M_p$ to their true values with respect to a given ranking (determined in step 3 of the simulation procedure) rather than the optimal ranking. We also compared $\log_{10} M_p$ estimates to $\log_{10} M_p^*$ (reflecting the optimal ranking). As expected, the magnitude of the difference increased as u decreased. For example, the difference between the estimates value of $\log_{10} M_{50\%}$ and $\log_{10} M_{50\%}^*$ was 0.02 for u=1, 0.02 for u=0.75, 0.04 for u=0.5, 0.11 for u=0.25, and 2.9 for u=0 (Supplementary Table 29).

We performed six secondary analyses. First, we repeated the analysis using a version of S-LDSC that does not constrain per-SNP heritabilities to be non-negative. The results were similar (Supplementary Table 29), but interpretation was more challenging because some per-SNP heritability estimates became negative. Second, we varied the PolyFun sample size in the range 107K - 1 million and obtained qualitatively similar results (Supplementary Table 29). Third, we varied the SNP heritability in the range 12.5%-50% and obtained qualitatively similar results (Supplementary Table 29). Fourth, we varied the genome-wide proportion of causal SNPs in the range 0.1%-1% and obtained qualitatively similar results (Supplementary Table 29). Fifth, we varied the number of bins used for partitioning SNPs in the range 5-20 and obtained qualitatively similar results (Supplementary Table 29). Finally, we evaluated the results with respect to a ranking of SNPs based only on the magnitude of their summary statistics. We obtained highly conservative results with respect to both the true value of M_p and to M_p^* in all cases (Supplementary Table 30), demonstrating that accurate polygenic localization estimates require performing genome-wide fine-mapping rather than simply ranking SNPs based on their summary statistics.

Acknowledgements

We thank Bogdan Pasaniuc, Gleb Kichaev, Matthew Stephens, Gao Wang, and Masahiro Kanai for helpful discussions. This research was conducted using the UK Biobank Resource under Application #16549 and was funded by NIH grants U01 HG009379, R01 MH107649, R01 MH101244 and R01 HG006399 HG006399, and by the Academy of Finland grants 288509 and 312076. HKF is supported by Eric and Wendy Schmidt. Computational analyses were performed on the O2 High-Performance Compute Cluster at Harvard Medical School.

URLs

Software implementing PolyFun and PolyLoc will be released prior to publication as a publicly available, open-source software package: https://www.hsph.harvard.edu/alkes-price/software

Baseline-LF v2.2.UKB annotations and LD-scores for UK Biobank SNPs:
https://data.broadinstitute.org/alkesgroup/LDSCORE/baselineLF_v2.2.UKB.tar.gz

bioRxiv preprint doi: https://doi.org/10.1101/807792; this version posted October 29, 2019. The copyright holder for this preprint (which was not certified by peer review) is the author/funder, who has granted bioRxiv a license to display the preprint in perpetuity. It is made available under aCC-BY 4.0 International license.

Summary LD information of N=337K UK Biobank individuals for 2,673 overlapping 3Mb loci will be released prior to publication: https://data.broadinstitute.org/alkesgroup/UKBB_LD/

Fine-mapping results for all analyzed SNPs: https://data.broadinstitute.org/alkesgroup/polyfun_results/

SuSiE: https://github.com/stephenslab/susieR

FINEMAP: http://www.christianbenner.com/#

UK Biobank Resource: http://www.ukbiobank.ac.uk/

bioRxiv preprint doi: https://doi.org/10.1101/807792; this version posted October 29, 2019. The copyright holder for this preprint (which was not certified by peer review) is the author/funder, who has granted bioRxiv a license to display the preprint in perpetuity. It is made available under aCC-BY 4.0 International license.

References

1. Visscher, P. M. *et al.* 10 years of GWAS discovery: biology, function, and translation. *Am. J. Hum. Genet.* **101**, 5–22 (2017).
2. Shendure, J., Findlay, G. M. & Snyder, M. W. Genomic Medicine–Progress, Pitfalls, and Promise. *Cell* **177**, 45–57 (2019).
3. Schaid, D. J., Chen, W. & Larson, N. B. From genome-wide associations to candidate causal variants by statistical fine-mapping. *Nat Rev Genet* **19**, 491–504 (2018).
4. The Wellcome Trust Case Control Consortium *et al.* Bayesian refinement of association signals for 14 loci in 3 common diseases. *Nat. Genet.* **44**, 1294–1301 (2012).
5. Hormozdiari, F., Kostem, E., Kang, E. Y., Pasaniuc, B. & Eskin, E. Identifying causal variants at loci with multiple signals of association. *Genetics* **198**, 497–508 (2014).
6. Chen, W. *et al.* Fine mapping causal variants with an approximate Bayesian method using marginal test statistics. *Genetics* **200**, 719–736 (2015).
7. Farh, K. K.-H. *et al.* Genetic and epigenetic fine mapping of causal autoimmune disease variants. *Nature* **518**, 337 (2015).
8. Huang, H. *et al.* Fine-mapping inflammatory bowel disease loci to single-variant resolution. *Nature* **547**, 173–178 (2017).
9. Mahajan, A. *et al.* Refining the accuracy of validated target identification through coding variant fine-mapping in type 2 diabetes. *Nat. Genet.* **50**, 559 (2018).
10. Mahajan, A. *et al.* Fine-mapping type 2 diabetes loci to single-variant resolution using high-density imputation and islet-specific epigenome maps. *Nat. Genet.* **50**, 1505 (2018).
11. Westra, H.-J. *et al.* Fine-mapping and functional studies highlight potential causal variants for rheumatoid arthritis and type 1 diabetes. *Nat. Genet.* **50**, 1366–1374 (2018).

bioRxiv preprint doi: https://doi.org/10.1101/807792; this version posted October 29, 2019. The copyright holder for this preprint (which was not certified by peer review) is the author/funder, who has granted bioRxiv a license to display the preprint in perpetuity. It is made available under aCC-BY 4.0 International license.

12. Ulirsch, J. C. *et al.* Interrogation of human hematopoiesis at single-cell and single-variant resolution. *Nat. Genet.* (2019) doi:10.1038/s41588-019-0362-6.

13. Maurano, M. T. *et al.* Systematic Localization of Common Disease-Associated Variation in Regulatory DNA. *Science* **337**, 1190–1195 (2012).

14. The ENCODE Project Consortium. An integrated encyclopedia of DNA elements in the human genome. *Nature* **489**, 57–74 (2012).

15. Trynka, G. *et al.* Chromatin marks identify critical cell types for fine mapping complex trait variants. *Nat. Genet.* **45**, 124 (2013).

16. The Roadmap Epigenomics Consortium. Integrative analysis of 111 reference human epigenomes. *Nature* **518**, 317–330 (2015).

17. Finucane, H. K. *et al.* Partitioning heritability by functional annotation using genome-wide association summary statistics. *Nat. Genet.* **47**, 1228–1235 (2015).

18. Kichaev, G. *et al.* Integrating Functional Data to Prioritize Causal Variants in Statistical Fine-Mapping Studies. *PLoS Genet.* **10**, e1004722 (2014).

19. Kichaev, G. *et al.* Improved methods for multi-trait fine mapping of pleiotropic risk loci. *Bioinformatics* **33**, 248–255 (2017).

20. Chen, W., McDonnell, S. K., Thibodeau, S. N., Tillmans, L. S. & Schaid, D. J. Incorporating functional annotations for fine-mapping causal variants in a Bayesian framework using summary statistics. *Genetics* **204**, 933–958 (2016).

21. Pickrell, J. K. Joint Analysis of Functional Genomic Data and Genome-wide Association Studies of 18 Human Traits. *Am. J. Hum. Genet.* **94**, 559–573 (2014).

22. Wang, G., Sarkar, A. K., Carbonetto, P. & Stephens, M. A simple new approach to variable selection in regression, with application to genetic fine-mapping. *bioRxiv* 501114 (2018).

bioRxiv preprint doi: https://doi.org/10.1101/807792; this version posted October 29, 2019. The copyright holder for this preprint (which was not certified by peer review) is the author/funder, who has granted bioRxiv a license to display the preprint in perpetuity. It is made available under aCC-BY 4.0 International license.

23. Benner, C. *et al.* FINEMAP: efficient variable selection using summary data from genome-wide association studies. *Bioinformatics* **32**, 1493–1501 (2016).

24. Benner, C., Havulinna, A., Salomaa, V., Ripatti, S. & Pirinen, M. Refining fine-mapping: effect sizes and regional heritability. *bioRxiv* 318618 (2018).

25. Gazal, S. *et al.* Linkage disequilibrium–dependent architecture of human complex traits shows action of negative selection. *Nat. Genet.* **49**, 1421–1427 (2017).

26. Gazal, S. *et al.* Functional architecture of low-frequency variants highlights strength of negative selection across coding and non-coding annotations. *Nat. Genet.* **50**, 1600–1607 (2018).

27. Gazal, S., Marquez-Luna, C., Finucane, H. K. & Price, A. L. Reconciling S-LDSC and LDAK functional enrichment estimates. *Nat. Genet.* **51**, 1202–1204 (2019).

28. Bycroft, C. *et al.* The UK Biobank resource with deep phenotyping and genomic data. *Nature* **562**, 203 (2018).

29. O'Connor, L. J. *et al.* Extreme Polygenicity of Complex Traits Is Explained by Negative Selection. *Am. J. Hum. Genet.* **105**, 456–476 (2019).

30. Benner, C. *et al.* Prospects of Fine-Mapping Trait-Associated Genomic Regions by Using Summary Statistics from Genome-wide Association Studies. *Am. J. Hum. Genet.* **101**, 539–551 (2017).

31. Benjamini, Y. & Hochberg, Y. Controlling the false discovery rate: a practical and powerful approach to multiple testing. *J. R. Stat. Soc. Ser. B Methodol.* **57**, 289–300 (1995).

32. Storey, J. D. & Tibshirani, R. Statistical significance for genomewide studies. *Proc. Natl. Acad. Sci.* **100**, 9440–9445 (2003).

33. Li, Y. I. *et al.* RNA splicing is a primary link between genetic variation and disease. *Science* **352**, 600–604 (2016).

34. Marquez-Luna, C. *et al.* Modeling functional enrichment improves polygenic prediction accuracy in UK Biobank and 23andMe data sets. *bioRxiv* 375337 (2018).

bioRxiv preprint doi: https://doi.org/10.1101/807792; this version posted October 29, 2019. The copyright holder for this preprint (which was not certified by peer review) is the author/funder, who has granted bioRxiv a license to display the preprint in perpetuity. It is made available under aCC-BY 4.0 International license.

35. Loh, P.-R., Kichaev, G., Gazal, S., Schoech, A. P. & Price, A. L. Mixed-model association for biobank-scale datasets. *Nat. Genet.* **50**, 906–908 (2018).

36. Park, J. H. *et al.* SLC39A8 deficiency: a disorder of manganese transport and glycosylation. *Am. J. Hum. Genet.* **97**, 894–903 (2015).

37. Li, D. *et al.* A pleiotropic missense variant in SLC39A8 is associated with Crohn's disease and human gut microbiome composition. *Gastroenterology* **151**, 724–732 (2016).

38. Bierut, L. J. *et al.* ADH1B is associated with alcohol dependence and alcohol consumption in populations of European and African ancestry. *Mol. Psychiatry* **17**, 445 (2012).

39. Mirzaa, G. M. *et al.* De novo CCND2 mutations leading to stabilization of cyclin D2 cause megalencephaly-polymicrogyria-polydactyly-hydrocephalus syndrome. *Nat. Genet.* **46**, 510 (2014).

40. Pickrell, J. K. *et al.* Detection and interpretation of shared genetic influences on 42 human traits. *Nat. Genet.* **48**, 709 (2016).

41. Hujoel, M. L., Gazal, S., Hormozdiari, F., van de Geijn, B. & Price, A. L. Disease heritability enrichment of regulatory elements is concentrated in elements with ancient sequence age and conserved function across species. *Am. J. Hum. Genet.* **104**, 611–624 (2019).

42. Claussnitzer, M. *et al.* FTO obesity variant circuitry and adipocyte browning in humans. *N. Engl. J. Med.* **373**, 895–907 (2015).

43. Jung, I. *et al.* A compendium of promoter-centered long-range chromatin interactions in the human genome. *Nat. Genet.* 1–8 (2019).

44. Zeggini, E., Gloyn, A. L., Barton, A. C. & Wain, L. V. Translational genomics and precision medicine: Moving from the lab to the clinic. *Science* **365**, 1409–1413 (2019).

45. Zeng, J. *et al.* Signatures of negative selection in the genetic architecture of human complex traits. *Nat. Genet.* **50**, 746 (2018).

bioRxiv preprint doi: https://doi.org/10.1101/807792; this version posted October 29, 2019. The copyright holder for this preprint (which was not certified by peer review) is the author/funder, who has granted bioRxiv a license to display the preprint in perpetuity. It is made available under aCC-BY 4.0 International license.

46. Zhang, Y., Qi, G., Park, J.-H. & Chatterjee, N. Estimation of complex effect-size distributions using summary-level statistics from genome-wide association studies across 32 complex traits. *Nat. Genet.* **50**, 1318 (2018).

47. Zhu, X. & Stephens, M. Large-scale genome-wide enrichment analyses identify new trait-associated genes and pathways across 31 human phenotypes. *Nat. Commun.* **9**, 4361 (2018).

48. Moser, G. *et al.* Simultaneous discovery, estimation and prediction analysis of complex traits using a Bayesian mixture model. *PLoS Genet* **11**, e1004969 (2015).

49. Schoech, A. P. *et al.* Quantification of frequency-dependent genetic architectures in 25 UK Biobank traits reveals action of negative selection. *Nat. Commun.* **10**, 790 (2019).

50. Yang, J. *et al.* Genetic variance estimation with imputed variants finds negligible missing heritability for human height and body mass index. *Nat. Genet.* **47**, 1114–20 (2015).

51. Purcell, S. M. *et al.* Common polygenic variation contributes to risk of schizophrenia and bipolar disorder. *Nature* **460**, 748–752 (2009).

52. Yang, J. *et al.* Common SNPs explain a large proportion of the heritability for human height. *Nat. Genet.* **42**, 565–569 (2010).

53. Loh, P.-R. *et al.* Contrasting genetic architectures of schizophrenia and other complex diseases using fast variance-components analysis. *Nat. Genet.* **47**, 1385–1392 (2015).

54. Boyle, E. A., Li, Y. I. & Pritchard, J. K. An Expanded View of Complex Traits: From Polygenic to Omnigenic. *Cell* **169**, 1177–1186 (2017).

55. Chatterjee, N., Shi, J. & García-Closas, M. Developing and evaluating polygenic risk prediction models for stratified disease prevention. *Nat. Rev. Genet.* **17**, 392–406 (2016).

56. Márquez-Luna, C., Loh, P.-R., South Asian Type 2 Diabetes (SAT2D) Consortium, The SIGMA Type 2 Diabetes Consortium & Price, A. L. Multiethnic polygenic risk scores improve risk prediction in diverse populations. *Genet. Epidemiol.* **41**, 811–823 (2017).

bioRxiv preprint doi: https://doi.org/10.1101/807792; this version posted October 29, 2019. The copyright holder for this preprint (which was not certified by peer review) is the author/funder, who has granted bioRxiv a license to display the preprint in perpetuity. It is made available under aCC-BY 4.0 International license.

57. Martin, A. R. *et al.* Clinical use of current polygenic risk scores may exacerbate health disparities. *Nat. Genet.* **51**, 584 (2019).

58. Solovieff, N., Cotsapas, C., Lee, P. H., Purcell, S. M. & Smoller, J. W. Pleiotropy in complex traits: challenges and strategies. *Nat. Rev. Genet.* **14**, 483 (2013).

59. Wang, K., Li, M. & Hakonarson, H. Analysing biological pathways in genome-wide association studies. *Nat. Rev. Genet.* **11**, 843 (2010).

60. De Leeuw, C. A., Neale, B. M., Heskes, T. & Posthuma, D. The statistical properties of gene-set analysis. *Nat. Rev. Genet.* **17**, 353 (2016).

61. Pasaniuc, B. & Price, A. L. Dissecting the genetics of complex traits using summary association statistics. *Nat. Rev. Genet.* **18**, 117–127 (2017).

62. Haworth, S. *et al.* Apparent latent structure within the UK Biobank sample has implications for epidemiological analysis. *Nat. Commun.* **10**, 333 (2019).

63. Van Hout, C. V. *et al.* Whole exome sequencing and characterization of coding variation in 49,960 individuals in the UK Biobank. *bioRxiv* 572347 (2019).

64. Zhong, H. & Prentice, R. L. Bias-reduced estimators and confidence intervals for odds ratios in genome-wide association studies. *Biostatistics* **9**, 621–634 (2008).

65. Ferguson, J. P., Cho, J. H., Yang, C. & Zhao, H. Empirical Bayes correction for the Winner's Curse in genetic association studies. *Genet. Epidemiol.* **37**, 60–68 (2013).

66. Kichaev, G. & Pasaniuc, B. Leveraging functional-annotation data in trans-ethnic fine-mapping studies. *Am. J. Hum. Genet.* **97**, 260–271 (2015).

67. Wang, H. & Song, M. Ckmeans.1d.dp: Optimal k-means Clustering in One Dimension by Dynamic Programming. *R J.* **3**, 29–33 (2011).

68. Reshef, Y. A. *et al.* Detecting genome-wide directional effects of transcription factor binding on polygenic disease risk. *Nat. Genet.* **50**, 1483 (2018).

bioRxiv preprint doi: https://doi.org/10.1101/807792; this version posted October 29, 2019. The copyright holder for this preprint (which was not certified by peer review) is the author/funder, who has granted bioRxiv a license to display the preprint in perpetuity. It is made available under aCC-BY 4.0 International license.

69. Hagberg, A., Swart, P. & S Chult, D. Exploring network structure, dynamics, and function using NetworkX. in *Proceedings of the 7th Python in Science Conference (SciPy2008)* (Los Alamos National Lab.(LANL), Los Alamos, NM (United States), 2008).

70. Shi, H., Kichaev, G. & Pasaniuc, B. Contrasting the Genetic Architecture of 30 Complex Traits from Summary Association Data. *Am. J. Hum. Genet.* **99**, 139–53 (2016).

71. Price, A. L. *et al.* Long-range LD can confound genome scans in admixed populations. *Am. J. Hum. Genet.* **83**, 132–135 (2008).

72. Wolfe, D., Dudek, S., Ritchie, M. D. & Pendergrass, S. A. Visualizing genomic information across chromosomes with PhenoGram. *BioData Min.* **6**, 18 (2013).

73. Bulik-Sullivan, B. K. *et al.* LD Score regression distinguishes confounding from polygenicity in genome-wide association studies. *Nat. Genet.* **47**, 291–295 (2015).

74. Welter, D. *et al.* The NHGRI GWAS Catalog, a curated resource of SNP-trait associations. *Nucleic Acids Res* **42**, D1001–D1006 (2014).

bioRxiv preprint doi: https://doi.org/10.1101/807792; this version posted October 29, 2019. The copyright holder for this preprint (which was not certified by peer review) is the author/funder, who has granted bioRxiv a license to display the preprint in perpetuity. It is made available under aCC-BY 4.0 International license.

Tables

Table 1: Summary of methods evaluated in simulations. For each method we report whether it incorporates functional data, the maximum number of functional annotations that we specified under default simulation settings (for fastPAINTOR we selected the number of annotations that maximized power while maintaining correct calibration; Methods), the maximum number of causal SNPs modeled per locus (or the exact number for SuSiE and PolyFun + SuSiE), and the corresponding reference. For fastPAINTOR and CAVIARBF, − denotes the exclusion of functional data. For CAVIARBF, 1 or 2 denotes the maximum number of causal variants. PolyFun + FINEMAP uses a new version of FINEMAP that we introduce here that incorporates prior causal probabilities.

Method	Functional data	Max #annotations	Max #causal SNPs	Ref.
fastPAINTOR−	No	N/A	Unlimited	[19]
fastPAINTOR	Yes	10	Unlimited	[19]
CAVIARBF1−	No	N/A	1	[6]
CAVIARBF1	Yes	Unlimited	1	[20]
CAVIARBF2−	No	N/A	2	[6]
CAVIARBF2	Yes	Unlimited	2	[20]
FINEMAP	No	N/A	10	[23,24]
PolyFun + FINEMAP	Yes	Unlimited	10	This paper
SuSiE	No	N/A	10	[22]
PolyFun + SuSiE	Yes	Unlimited	10	This paper

bioRxiv preprint doi: https://doi.org/10.1101/807792; this version posted October 29, 2019. The copyright holder for this preprint (which was not certified by peer review) is the author/funder, who has granted bioRxiv a license to display the preprint in perpetuity. It is made available under aCC-BY 4.0 International license.

Table 2: Pleiotropic fine-mapped SNPs for UK Biobank traits. We report SNPs fine-mapped (PIP>0.95) for ≥4 genetically uncorrelated traits ($|r_g|$<0.2). For each SNP we report its name (SNP), position (hg19), MAF in the UK Biobank, closest gene(s) (using data from the GWAS catalog[74]), top annotation (Methods) and fine-mapped traits (and the number of fine-mapped traits). SNPs are ordered first by the number of fine-mapped traits and then by genomic position. HDL: HDL cholesterol; MC: monocyte count; MPV: mean platelet volume; HLSRC: high light scatter reticulocyte count; Cholesterol: total cholesterol; RBCDW: red blood cell distribution width; FEV1/FVC: ratio of forced expiratory volume to forced vital capacity; MCH: mean corpuscular hemoglobin; SBP: systolic blood pressure; DBP: diastolic blood pressure; FVC: forced vital capacity; Cardiovascular: cardiovascular-related disease; RBC: red blood cell count; LC: lymphocyte count; HbA1c: Hemoglobin A1c; WHR: waist-hip ratio (adjusted for BMI). Results for all 223 pleiotropic fine-mapped SNPs are reported in Supplementary Table 12.

SNP	Position	MAF	Closest gene(s)	Annotation	Traits
rs13107325	chr4:103188709	0.08	SLC39A8	non-synonymous	BMI, Balding, Cholesterol, DBP, FVC, Height, RBC, WHR (8)
rs1229984	chr4:100239319	0.02	ADH1B	non-synonymous	BMI, LDL, MCH, MPV, SBP, Vitamin D (6)
rs76895963	chr12:4384844	0.02	CCND2,CCND2-AS1	Conserved	BMD, Height, RBC, SBP, Triglycerides (5)
rs140584594	chr1:110232983	0.27	GSTM1	non-synonymous	HDL, Height, MC, MPV (4)
rs3811444	chr1:248039451	0.33	TRIM58	non-synonymous	HLSRC, HbA1c, Platelet Count, RBC (4)
rs1260326	chr2:27730940	0.39	GCKR	non-synonymous	Cholesterol, Height, Platelet Count, RBCDW (4)
rs2270894	chr3:9975386	0.2	CRELD1,IL17RC	Conserved	BMD, FEV1/FVC, Height, Platelet Count (4)
rs11556924	chr7:129663496	0.39	ZC3HC1	non-synonymous	Age Menarche, Cardiovascular, Height, Platelet Count (4)
rs3918226	chr7:150690176	0.08	NOS3	Conserved	Eczema, Height, High Cholesterol, MPV (4)
rs150813342	chr9:135864513	0.01	GFI1B	Conserved	Eosinophil Count, HLSRC, MCH, Platelet Count (4)
rs964184	chr11:116648917	0.13	ZPR1	DHS	Cholesterol, MPV, RBCDW, Vitamin D (4)
rs35979828	chr12:54685880	0.07	NFE2	Conserved	Eosinophil Count, Platelet Count, RBC, RBCDW (4)
rs2277339	chr12:57146069	0.1	PRIM1	non-synonymous	Height, LC, RBC, RBCDW (4)
rs72681869	chr14:50655357	0.01	SOS2	non-synonymous	FVC, Hair Color, HbA1c, SBP (4)
rs61745086	chr16:88782050	0.01	PIEZO1,CTU2	non-synonymous	HLSRC, HbA1c, Height, RBC (4)
rs34557412	chr17:16852187	0.01	TNFRSF13B	non-synonymous	HbA1c, MC, MPV, RBC (4)
rs77542162	chr17:67081278	0.02	ABCA6	non-synonymous	HbA1c, Height, LDL, Platelet Count (4)

bioRxiv preprint doi: https://doi.org/10.1101/807792; this version posted October 29, 2019. The copyright holder for this preprint (which was not certified by peer review) is the author/funder, who has granted bioRxiv a license to display the preprint in perpetuity. It is made available under aCC-BY 4.0 International license.

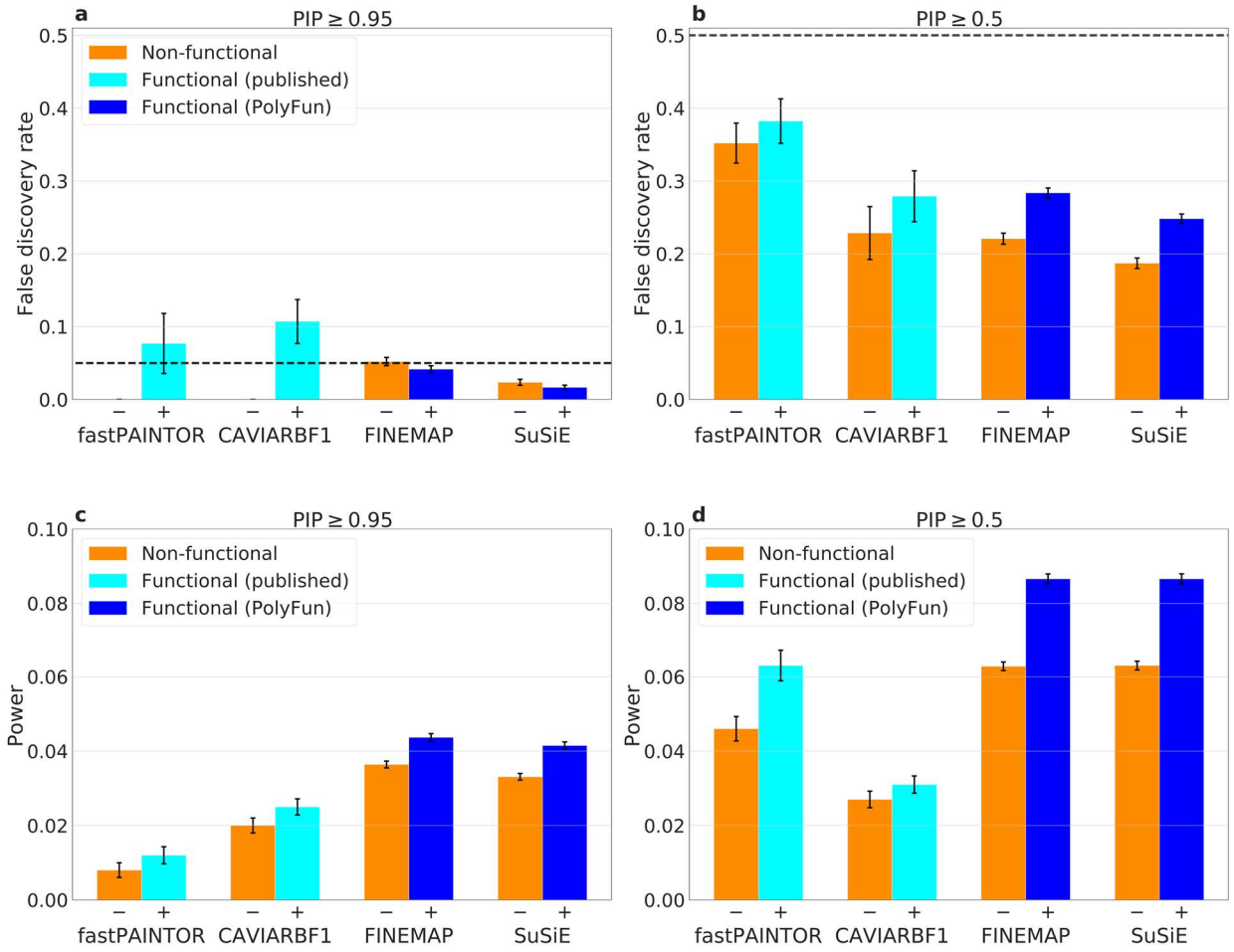

Figure 1: Calibration and power of fine-mapping methods in simulations. (**a**-**b**) False discovery rates at PIP=0.95 (a) and PIP=0.5 (b). Dashed horizontal lines denote conservative estimates of false discovery rates (Methods). (**c**-**d**) Power at PIP=0.95 (c) and PIP=0.5 (d). The first bar of each method uses non-functionally informed fine-mapping (denoted −), and the second uses functionally informed fine-mapping (denoted +). Error bars denote standard errors. Exact false-discovery thresholds are reported in Supplementary Figure 1. Numerical results, including results for CAVIARBF2− and CAVIARBF2, are reported in Supplementary Table 4.

bioRxiv preprint doi: https://doi.org/10.1101/807792; this version posted October 29, 2019. The copyright holder for this preprint (which was not certified by peer review) is the author/funder, who has granted bioRxiv a license to display the preprint in perpetuity. It is made available under aCC-BY 4.0 International license.

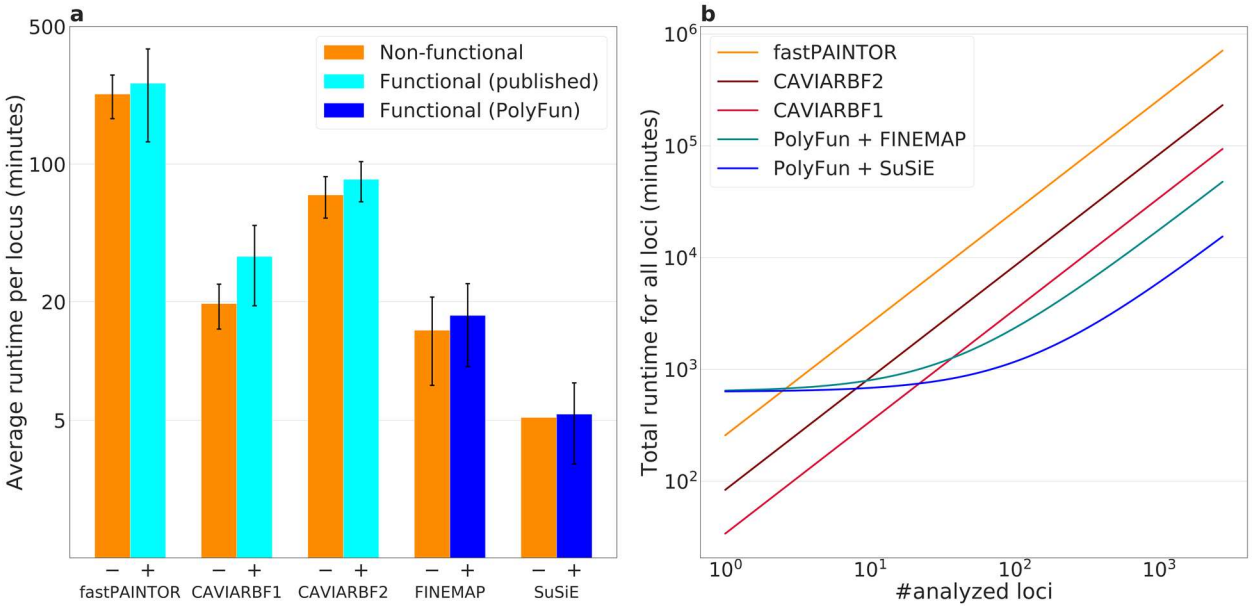

Figure 2: Computational cost of fine-mapping methods. (**a**) The average runtime required to fine-map a 3Mb locus in a genome-wide analysis (log scale). The first bar of each method uses non-functionally informed fine-mapping (denoted −), and the second uses functionally informed fine-mapping (denoted +). (**b**) The total runtime required to fine-map different numbers of loci, for functionally informed fine-mapping methods only (log scale). The runtimes of PolyFun + SuSiE and PolyFun + FINEMAP are sub-linear because they include the fixed preprocessing cost of computing prior causal probabilities (630 minutes). Numerical results, including panel (b) results for non-functionally informed methods, are reported in Supplementary Table 4.

bioRxiv preprint doi: https://doi.org/10.1101/807792; this version posted October 29, 2019. The copyright holder for this preprint (which was not certified by peer review) is the author/funder, who has granted bioRxiv a license to display the preprint in perpetuity. It is made available under aCC-BY 4.0 International license.

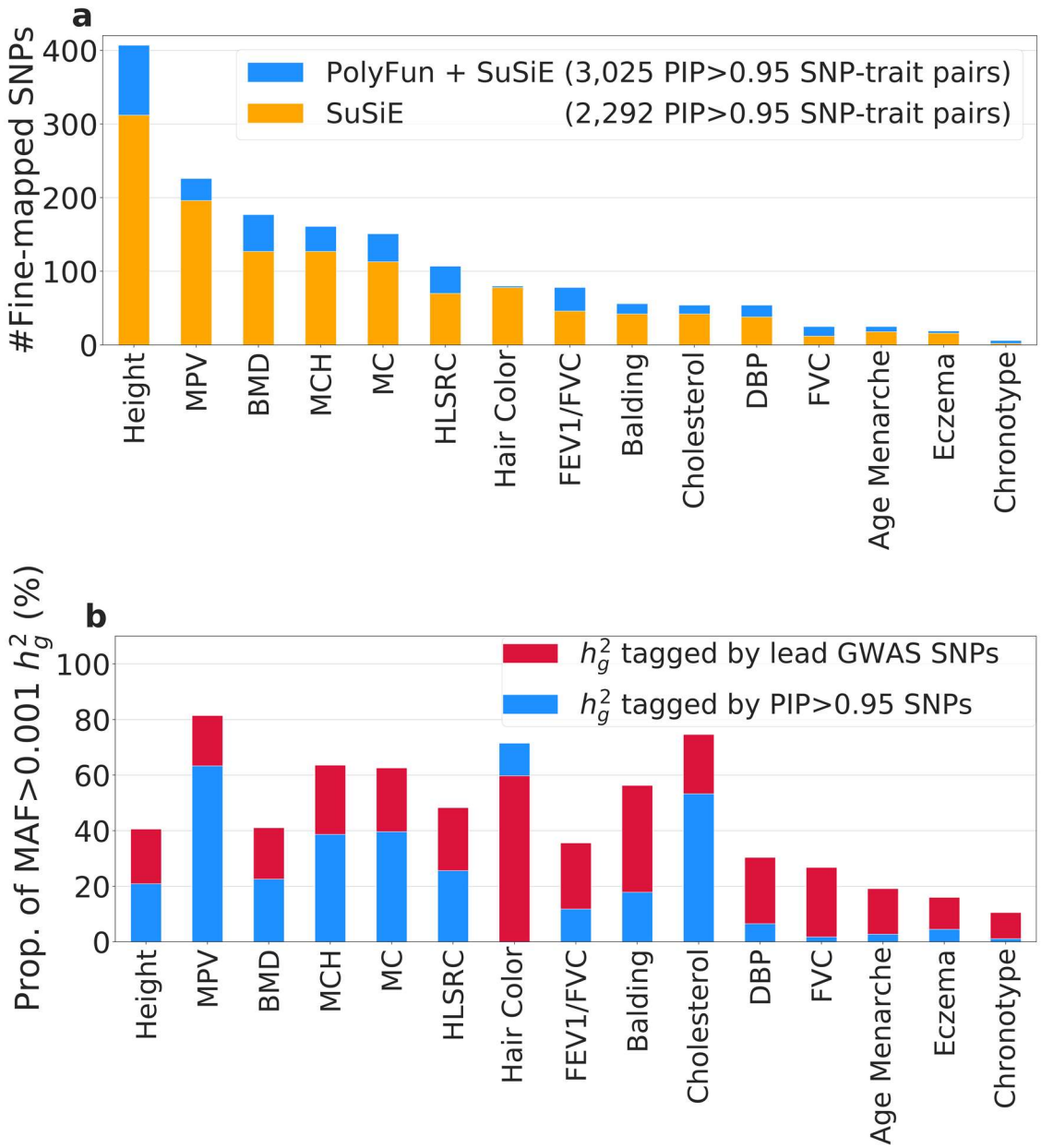

Figure 3: Summary of fine-mapping results for UK Biobank traits. (**a**) the number of SNPs with PIP>0.95 identified by SuSiE (orange bars) and PolyFun + SuSiE (blue bars) across 15 genetically uncorrelated traits in the UK Biobank. Traits are ordered by PolyFun + SuSiE results. The numbers in the legend refer to the sum of all 47 traits analyzed. (**b**) The proportion of MAF>0.001 SNP-heritability (h_g^2) tagged by lead GWAS SNPs (crimson bars) and by PolyFun + SuSiE PIP>0.95 SNPs (blue bars). Traits are ordered as in panel (a). For hair color, the h_g^2 tagged by PIP>0.95 SNPs is greater than h_g^2 tagged by lead GWAS SNPs. MPV: Mean platelet volume; BMD: bone mineral density; MCH: mean corpuscular hemoglobin; MC: monocyte count; HLSRC: high light scatter reticulocyte count; FEV1/FVC: ratio of forced expiratory volume to forced vital capacity; DBP: diastolic blood pressure; FVC: forced vital capacity. Numerical results are reported in Supplementary Tables 6,11.

bioRxiv preprint doi: https://doi.org/10.1101/807792; this version posted October 29, 2019. The copyright holder for this preprint (which was not certified by peer review) is the author/funder, who has granted bioRxiv a license to display the preprint in perpetuity. It is made available under aCC-BY 4.0 International license.

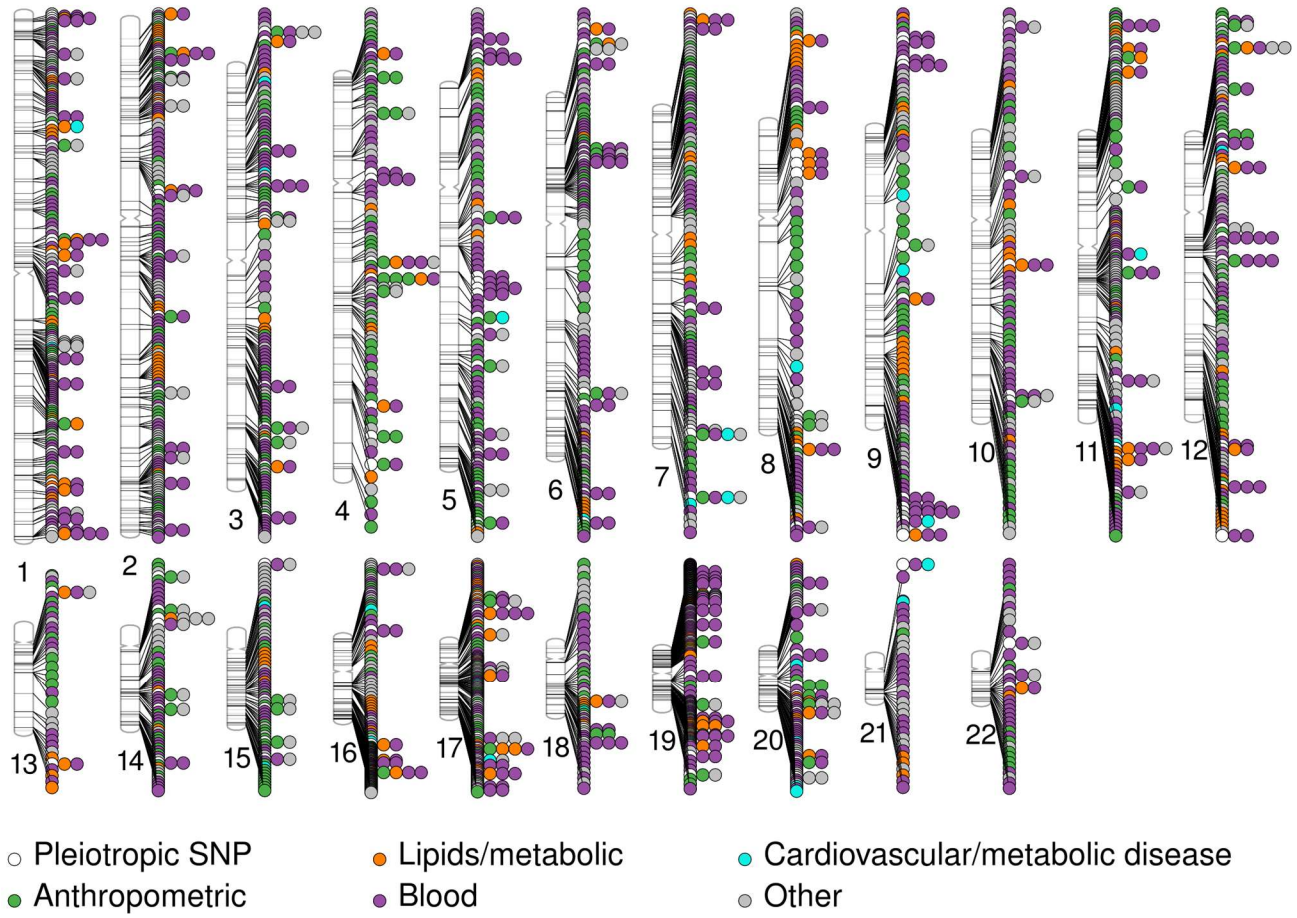

Figure 4: **Visualization of fine-mapping results for UK Biobank traits**. We display an ideogram of all 2,225 PIP>0.95 fine-mapped SNPs identified by PolyFun + SuSiE across 47 UK Biobank traits. Traits are color-coded into groups (see legend and Supplementary Table 5). White circles indicate SNPs that are pleiotropic for ≥2 genetically uncorrelated traits, with circles to the right of a white circle denoting the genetically uncorrelated traits (max of 5 colored circles due to space limitations). Numerical results are reported in Supplementary Table 7.

bioRxiv preprint doi: https://doi.org/10.1101/807792; this version posted October 29, 2019. The copyright holder for this preprint (which was not certified by peer review) is the author/funder, who has granted bioRxiv a license to display the preprint in perpetuity. It is made available under aCC-BY 4.0 International license.

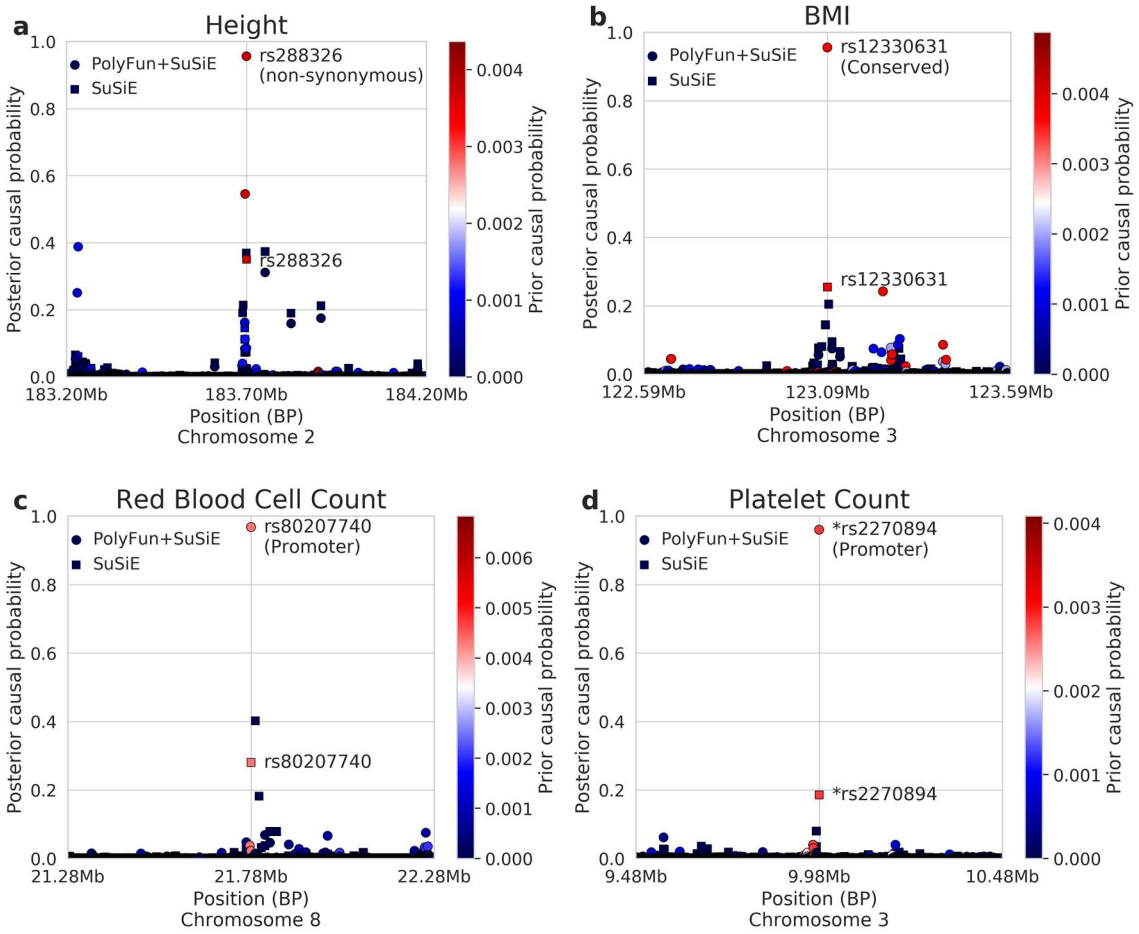

Figure 5: Examples of the advantages of functionally-informed fine-mapping for UK Biobank traits. We report four examples where PolyFun + SuSiE identified a fine-mapped common SNP (PIP>0.95) but SuSiE did not (PIP<0.5 for all SNPs within 1Mb). Circles denote PolyFun + SuSiE PIPs and squares denote SuSiE PIPs. SNPs are shaded according to their prior causal probabilities estimated by PolyFun. The top PolyFun + SuSiE SNP is labeled (next to its PolyFun + SuSiE PIP and its SuSiE PIP). The annotation of each top PolyFun + SuSiE SNP that is most enriched among SuSiE PIP>0.95 SNPs (Methods) is reported in parentheses below its label. Asterisks denote lead GWAS SNPs. Numerical results are reported in Supplementary Table 13.

bioRxiv preprint doi: https://doi.org/10.1101/807792; this version posted October 29, 2019. The copyright holder for this preprint (which was not certified by peer review) is the author/funder, who has granted bioRxiv a license to display the preprint in perpetuity. It is made available under aCC-BY 4.0 International license.

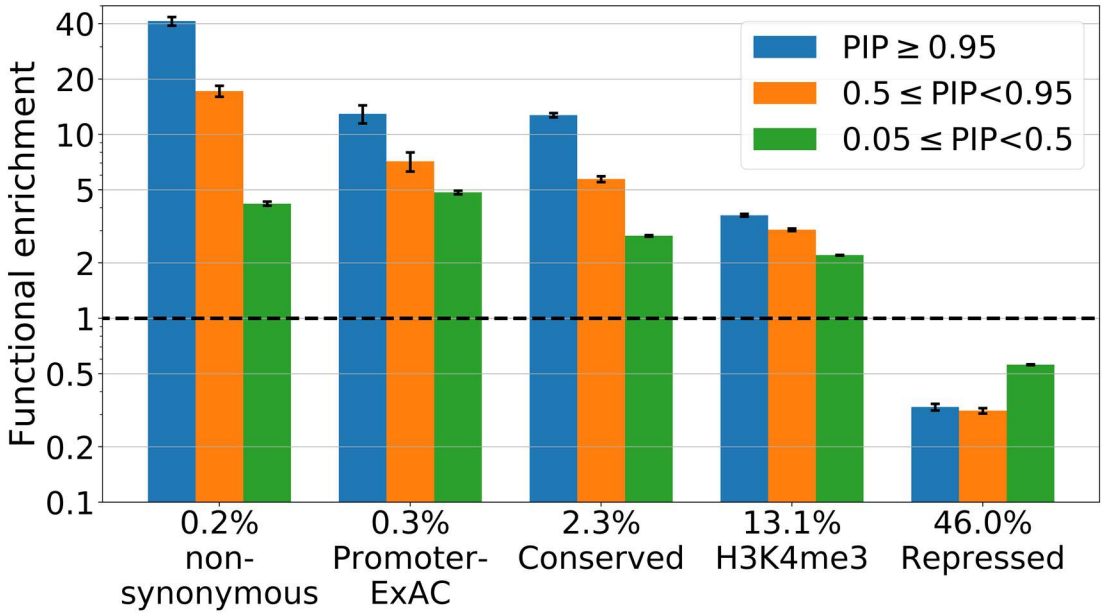

Figure 6: Functional enrichment of SuSiE fine-mapped common SNPs for UK Biobank traits. We report the functional enrichment of fine-mapped common SNPs (defined as the proportion of common SNPs in a PIP range lying in an annotation divided by the proportion of genome-wide common SNPs lying in the annotation) for 5 selected binary annotations, meta-analyzed across 14 genetically uncorrelated UK Biobank traits with ≥10 PIP>0.95 SNPs (log scale). The proportion of common SNPs lying in each binary annotation is reported above its name. The horizontal dashed line denotes no enrichment. Error bars denote standard errors. Numerical results for all 50 main binary annotations and all traits are reported in Supplementary Table 14.

bioRxiv preprint doi: https://doi.org/10.1101/807792; this version posted October 29, 2019. The copyright holder for this preprint (which was not certified by peer review) is the author/funder, who has granted bioRxiv a license to display the preprint in perpetuity. It is made available under aCC-BY 4.0 International license.

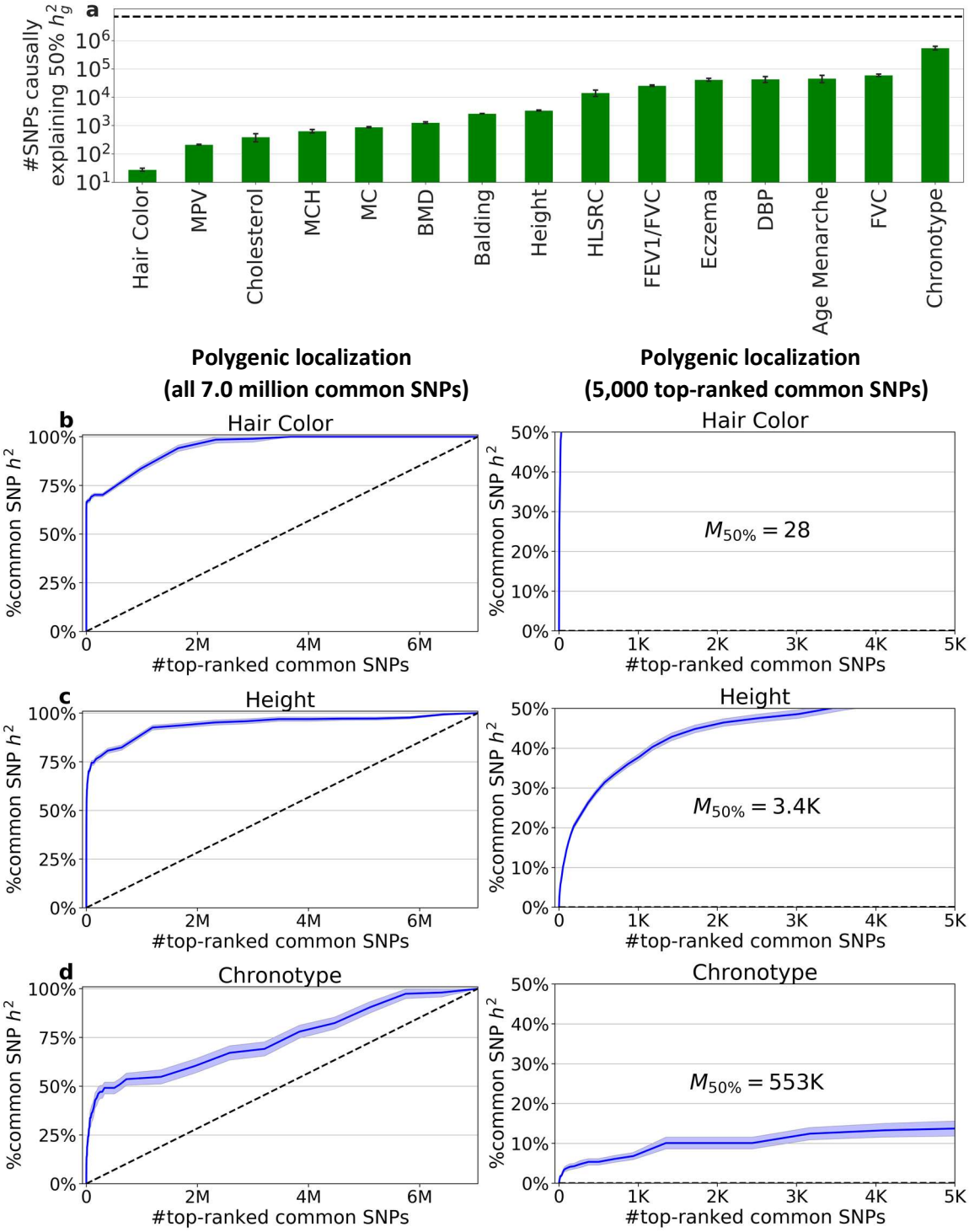

Figure 7: Polygenic localization results for UK Biobank traits. (a) $M_{50\%}$ estimates across 15 genetically uncorrelated traits. For each trait, we report the number of top-ranked common SNPs (using PolyFun + SuSiE posterior per-SNP heritability estimates for ranking) causally explaining 50% of common SNP heritability, and its standard error (log scale). The horizontal dashed line denotes the total number of common SNPs in the analysis (7.0 million). (**b**-**d**) The proportion of common SNP heritability of (b) hair color, (c) height, and (d) chronotype explained by different numbers of top-ranked SNPs, for all 7.0 million common SNPs (left) and the 5,000 top-ranked common (right). Purple shading denotes standard errors. Dashed black lines denote a null model with a constant per-SNP heritability. We also report the number of top-ranked SNPs causally explaining 50% of common SNP heritability, denoted $M_{50\%}$. Discontinuities in the slope indicate transitions between SNP bins. Numerical results for all 47 UK Biobank traits are reported in Supplementary Table 26.

bioRxiv preprint doi: https://doi.org/10.1101/807792; this version posted October 29, 2019. The copyright holder for this preprint (which was not certified by peer review) is the author/funder, who has granted bioRxiv a license to display the preprint in perpetuity. It is made available under aCC-BY 4.0 International license.